TOPICAL REVIEW • OPEN ACCESS

Free-energy orbital-free density functional theory: recent developments, perspective, and outlook

To cite this article: Valentin V Karasiev *et al* 2025 *Electron. Struct.* **7** 013001

IOP Publishing Electron. Struct. 7 (2025) 013001 https://doi.org/10.1088/2516-1075/adadd4

Electronic Structure

TOPICAL REVIEW

Free-energy orbital-free density functional theory: recent developments, perspective, and outlook

Valentin V Karasiev[1,*], **Katerina P Hilleke**[1] and **S B Trickey**[2]

[1] Laboratory for Laser Energetics, University of Rochester, 250 East River Road, Rochester, NY 14623, United States of America
[2] Quantum Theory Project, Departments of Physics and of Chemistry, University of Florida, Gainesville, FL 32611, United States of America
[*] Author to whom any correspondence should be addressed.

E-mail: vkarasev@lle.rochester.edu

Keywords: noninteracting free-energy, exchange-correlation free-energy, pseudo-potentials, orbital-free density functionals

OPEN ACCESS

RECEIVED
17 September 2024

REVISED
12 December 2024

ACCEPTED FOR PUBLICATION
23 January 2025

PUBLISHED
10 February 2025

Abstract

By summarizing the constraint-based development of orbital-free free-energy density functional approximations, we provide a perspective on progress over the last 15 years, the limitations of existing functionals, and the challenges awaiting resolution. We outline the chronology of the development of noninteracting and exchange-correlation free-energy orbital-free functionals and summarize the theoretical basis of existing local density approximation, second-order approximation, generalized gradient approximation (GGA), and meta-GGAs. We discuss limitations and challenges such as problems with thermodynamic derivatives, free-energy nonadditivity and the closely related issue of all-electron versus valence-only local pseudo-potential performance.

1. Setting

For predictive computational treatment of materials and their molecular ingredients, it is hardly an exaggeration to say that density functional theory [1–7] has been the single most influential theoretical innovation. This is not to denigrate explicit wave-function methods such as coupled-cluster theory and configuration interaction [8–12] but to emphasize the well-known fact that the scaling of their computational costs with the number of electrons N_e is quite high, typically $\mathcal{O}(N_e^6)$ or worse. There are better-scaling versions but, to our knowledge, they all exploit the existence of a gap or of sparsity, either explicitly or implicitly. For studies involving *both* metallic materials *and* molecular (or atomic) constituents, such improved scaling is of no avail. Explicit wave-function methods thus are almost always prohibitively costly unless the scope of the study is restricted severely.

It is perhaps less-well appreciated that somewhat the same issue increasingly distinguishes DFT usage in materials physics from quantum chemistry. In quantum chemistry applications it is common to use exchange-correlation (XC) density functional approximations (DFAs) that depend upon the Kohn–Sham (KS) orbitals (or generalized KS orbitals; the distinction does not matter here). The B3LYP [13] DFA is the molecular exemplar. Use of DFAs with more complicated orbital-dependencies is not rare in chemistry. A careful discussion of the distinct computer cost disadvantage of such DFAs for materials simulations is in sections 2.2.21–23 of [14]. Essentially the issue is the cost scaling of orbital-independent DFAs. In ordinary KS calculations it is $\propto \mathcal{O}(N_e^3)$. Even single-determinant orbital dependence pushes that to $\propto \mathcal{O}(N_e^4)$. This sort of cost scaling is, of course, a well-known motivation for orbital-free DFT [15].

In the usual electronic structure context, state conditions typically go undiscussed. Almost all ordinary chemistry and much of materials physics is done at temperature T $\lesssim$ 2000 K ($\approx$ 0.172 eV) and $P \lesssim$ 1 kbar, i.e. at near-ambient conditions. A practical consequence is that the Fermi–Dirac occupation number distribution is a step function ($f_i = 1$ for $\varepsilon_i \leqslant \varepsilon_F$ and $f_i = 0$ otherwise). DFT calculations with electronic temperature equal to 0 K at such near-ambient conditions therefore generally are adequate.

Dramatically higher T and P occur, however, in some important system types. Giant planet and exo-planet interiors are one example [16]. Another is warm dense matter (WDM), a material regime on the

pathway to inertial confinement fusion (ICF) [17]. WDM can have a wide range of temperatures T ≈ 1−100 eV (with 1 eV = 11 604.5 K) and P up to several Mbar. Clearly this is a completely different state-condition domain.

High T and P implicates electron populations that are highly excited compared to the ground state but not so highly as to be treatable as a classical two-component plasma with quantum corrections. Given the success of *ab initio* molecular dynamics (AIMD) at chemically ordinary T and P, the obvious step for high T and P is to go to free-energy DFT [18] as the electronic structure driver of the AIMD. For simplicity, here we assume the ion temperature, T_i, is set independently and is irrelevant to the discussion.

With respect to ground-state DFT, it suffices to say that free-energy DFT differs in three basic ways. First, there are non-zero Fermi–Dirac occupations for bands above the Fermi level ($f_i > 0$, for $\varepsilon_i \geqslant \varepsilon_F$). Thus, the minimizing number density becomes temperature-dependent $n(\mathbf{r}, T)$. Second, the noninteracting kinetic energy $T_s[n]$ defined by the KS decomposition becomes the noninteracting free energy $\mathcal{F}_s[n;T] = \mathcal{T}_s[n;T]] - T\mathcal{S}_s[n;T]$, with $\mathcal{T}_s$ and $\mathcal{S}_s$ the temperature-dependent noninteracting kinetic energy and entropy respectively. Third, the XC energy becomes the XC free energy $\mathcal{F}_{xc}[n;T]$ with explicit T dependence as well as implicit from the density $n(T)$. Though the finite-T KS equation has the same form as in the ground-state, the XC potential obviously is the functional derivative of $\mathcal{F}_{xc}[n;T]$.

For computational studies, the addition of T to P and V (system volume) as system state parameters necessitates more simulations than in the ground state. Inexorably, however, going to free-energy DFT in conventional KS form worsens the cost-scaling because the number of numerically significant non-zero *f_i* and associated number of thermally occupied bands N_b that must be taken into account typically is much larger than the number of electrons, $N_b \gg N_e$. That leads to the high-T limit scaling $\propto \mathcal{O}(N^3T^3)$. Here N is the system size in terms of number of electrons, number of atoms, or system volume [19]. There have been and continue to be attempts to get around that enlarged burden [20–23]. The close structural and conceptual kinship of free-energy DFT and the ground-state form make it obvious that orbital-free DFT would bestow the same kind of near-linear scaling $\propto \mathcal{O}(N\ln N)$ benefits, irrespective of temperature [23, 24].

This paper focuses on progress in free-energy OF-DFT since 2012. For the earlier record see [25]. We write from the perspective of being developers of useful, constraint-based free-energy and OF-DFT functionals. Formal theory development, in that perspective, is largely motivated by or required by the functional development process [26]. Section 2 introduces the background and basis of free-energy OF-DFT. Section 3 describes approximate noninteracting free-energy orbital-free functionals starting from the simplest, Thomas–Fermi, and continuing with the generalized gradient approximation (GGA) and meta-GGA frameworks based on the second- and fourth-order finite-T gradient expansions respectively. That section is focused mostly on one-point (or semi-local) functionals. Non-local (two-point) functionals are discussed briefly at the beginning. The section also includes an example of the comparative performance of semi-local orbital-free functionals applied to the dense deuterium equation of state. Section 4 reviews progress on the development of XC free-energy orbital-free functionals compatible with both orbital-free and conventional (orbital-based) KS schemes. Three subsections review the development and status of free-energy local density approximation (LDA), GGA, and meta-GGA XC functionals, including some aspects and additional considerations not covered by the respective original publications. Section 5 discusses two issues for free-energy OF-DFT that are especially relevant for WDM applications: use of all-electron (AE) local pseudo-potentials (LPPs) as required at very high temperatures, and the related issue of nonadditivity of orbital-free noninteracting kinetic-/free-energy density functionals. Section 6 concludes the survey.

2. Basics

As with the ground state, there are two distinct tasks facing free-energy OF-DFT, to get adequate approximations for the noninteracting free energy $\mathcal{F}_s$ and for the XC free energy $\mathcal{F}_{xc}$. This implicates the obvious requirement that one either has appropriate ground-state OF-DFT T_s and E_{xc} functionals or else one must make the free-energy versions have accurate ground-state limits. Either way, ground-state OF-DFT development is directly involved. We proceed in that context.

Consider a system of N_e electrons in the external potential $v_{ext}(\{\mathbf{R}\};\mathbf{r})$ of ions at positions $\{\mathbf{R}\}$. At T = 0 K, assuming the conventional KS decomposition of the total electronic kinetic energy into the noninteracting term, $T_s[n]$, plus a remainder included in the XC $E_{xc}[n]$ term, the DFT total energy orbital-free density functional has the form

$$E[n] = T_s[n] + E_H[n] + E_{xc}[n] + \int n(\mathbf{r})\, v_{ext}(\mathbf{r})\, d\mathbf{r} + E_{ion}(\{\mathbf{R}\}), \quad (1)$$

where $E_H[n]$ is the Hartree repulsion, and $E_{ion}(\{\mathbf{R}\})$ is the ion-ion electrostatic repulsion.

At finite-T, the total energy equation (1) is replaced by the grand canonical potential of the system (explicit T-dependence is suppressed for simplicity)

$$\Omega[n] = \mathcal{F}[n] + \int n(\mathbf{r})\,\{v_{\text{ext}}(\mathbf{r}) - \mu\}\mathrm{d}\mathbf{r} + E_{\text{ion}}(\{\mathbf{R}\})\,, \tag{2}$$

with μ the chemical potential, and $\mathcal{F}[n]$ the universal free-energy functional

$$\mathcal{F}[n] = \mathcal{F}_{\text{s}}[n] + E_{\text{H}}[n] + \mathcal{F}_{\text{xc}}[n]\,. \tag{3}$$

The variational minimization of $\Omega[n]$ with respect to the electron density gives the single Euler–Lagrange equation

$$\frac{\delta\mathcal{F}_{\text{s}}[n]}{\delta n(\mathbf{r})} + \frac{\delta E_{\text{H}}[n]}{\delta n(\mathbf{r})} + \frac{\delta\mathcal{F}_{\text{xc}}[n]}{\delta n(\mathbf{r})} + v_{ext}(\mathbf{r}) \equiv \frac{\delta\mathcal{F}_{\text{s}}[n]}{\delta n(\mathbf{r})} + v_{\text{KS}}([n];\mathbf{r}) = \mu\,. \tag{4}$$

The first critical ingredient is a suitable approximation for $\mathcal{F}_{\text{s}}$, the counterpart to $T_s[n]$ in the ground state. The most widely used approximations have been finite-T Thomas–Fermi [27] and the second-order gradient approximation (SGA). Both are local (one-point) approximations based upon the homogeneous electron gas (HEG). The T = 0 K second-order gradient correction to TF was generalized to finite-T by Perrot [28] more than 40 years ago, while TF-based finite-T AIMD studies first appeared almost 30 years ago [42, 43]. Despite the fact that TF and SGA obviously are far from satisfactory on fundamental grounds, they continue to be used [44–47]. The deficiencies are non-trivial. Teller [48] proved that the zero-T limit of the TF functional has no bound systems. The SGA functional may fail to predict detectable energy minima for extended systems; examples are provided in [29, 49]. Moreover, the SGA functional may introduce divergences or numerical instabilities in the interstitial and asymptotic regions where the electron density decays exponentially, leading to exponential increase of the SGA effective enhancement factor. It is proportional to the square of the reduced density gradient s defined in equation (14) below. (Remark: Peculiarly, many finite-T TF or SGA-based papers state, incorrectly, that OF-DFT is *defined* by the use of those functionals.)

In 2012, Karasiev *et al* [29] presented a framework for generalizing a ground-state GGA KE density functional (KEDF) into a gradient-dependent $\mathcal{F}_{\text{s}}$, thereby connecting with modern ground-state OF-DFT. They demonstrated the workings and effectiveness of that scheme by use on their semi-empirical PBE2 GGA KEDF. A bit over a year later, VT84F, the first non-empirical, constraint-based finite-T GGA KEDF, was presented [30]. By construction it has both proper T = 0 K limiting behavior and large-T behavior. Below we discuss progress since.

The second critical ingredient in equations (2)–(4) is an orbital-free approximation to $\mathcal{F}_{\text{xc}}$. A common approach is to use the ground-state approximation (GSA). In it, the XC free energy is evaluated by use of a ground-state T-independent functional evaluated with the finite-T density $\mathcal{F}_{\text{xc}}[n;\mathrm{T}] \approx E_{\text{xc}}[n(\mathrm{T})]$. The approach obviously has only an implicit T dependence. Lacking explicit XC thermal effects, the GSA is a demonstrably unreliable approach in a range of thermodynamic conditions across the warm dense regime. See [36, 40, 50, 51] among others. Such discrepancies arise in part because the GSA completely misses the XC entropic contribution. The total entropy of the system therefore is given, incorrectly, by the noninteracting term alone. Poor description of other XC temperature effects can lead to large errors (up to 20% or so) in, for example, predicted equations of state (EOS), depending on the system and state conditions. See examples in [36]. The consequence is that such DFT/GSA data are thermodynamically inconsistent, for example, with path integral Monte Carlo (PIMC) results. In short, there can be qualitatively different behavior from a GSA as compared to a properly thermal XC approximation of the same level of refinement as to functional variables.

Below we describe developments of the thermal LDA, GGA, and additive meta-GGA XC functionals, and summarize recent efforts to remove orbital dependence from modern ground-state meta-GGA E_{xc} forms ('de-orbitalize' them) as the predicate to generalizing them to T > 0 K.

As guidance to the discussion that follows, the essential chronology of development of T = 0 K orbital-free free-energy functionals, $\mathcal{F}_{\text{s}}$ and $\mathcal{F}_{\text{xc}}$, is displayed in table 1. With recent developments of the meta-GGA formalism for noninteracting free-energy and XC free-energies, finite-T OF-DFT has reached the same level of structural refinement as ground-state OF-DFT.

3. Noninteracting free energy orbital-free functionals

As in the zero-T case, the noninteracting free-energy density functionals fall into three classes (i) one-point functionals consisting of local (i.e. Thomas–Fermi) and semi-local (GGA, meta-GGA); (ii) non-local

Table 1. Time line of modern noninteracting and XC orbital-free free-energy density functional development.

Year	Functional	Reference
1949	Thomas–Fermi $\mathcal{F}_s$	Feynman *et al* [27]
1979	Second-order gradient expansion $\mathcal{F}_s$	Perrot [28]
2012	GGA formalism for constructing $\mathcal{F}_s$	Karasiev *et al* [29]
2013	VT84F GGA $\mathcal{F}_s$	Karasiev *et al* [30]
2013	Non-local (2-point) $\mathcal{F}_s$	Sjostrom and Daligault [31]
2020	LKT GGA $\mathcal{F}_s$	Luo *et al* [32]
2024	Non-local (2-point) XWMF $\mathcal{F}_s$	Ma *et al* [33]
2024	meta-GGA formalism for constructing $\mathcal{F}_s$ & DEL and PGSLr meta-GGA $\mathcal{F}_s$	Karasiev *et al* [34]
2014	KSDT LDA $\mathcal{F}_{xc}$	Karasiev *et al* [35] (see [36] for the corrected corrKSDT version)
2014	Additive GGA $\mathcal{F}_{xc}$	Sjostrom and Daligault [37]
2017	GDSMFB LDA, minor corrections of KSDT LDA[a]	Groth *et al* [38, 39]
2018	KDT16 GGA $\mathcal{F}_{xc}$	Karasiev *et al* [36]
2022	Additive meta-GGA $\mathcal{F}_{xc}$	Karasiev *et al* [40]

[a] Refinement of KSDT XC to match improved Monte Carlo data for the homogeneous electron gas (HEG) at finite-T and correct a minor fitting error. The practical equivalence of GDSMFB to KSDT is discussed in detail in [41].

(two-point) functionals; and (iii) emerging machine-learnt free-energy functionals [52]. Besides their explicit temperature dependence, local and semi-local functionals depend on density (LDA rung), density and density gradient (GGA rung), and density, density gradients and density Laplacian (meta-GGA rung). (Remark: The 'rung' typology parallels the ground-state XC 'Jacob's ladder' introduced by Perdew and Schmidt [53].)

Here we focus discussion mostly upon one-point functionals. They have received far more attention because their form provides both ready enforcement of constraints and computational simplicity (which thereby broadens their applicability). However, a brief review of two-point finite-T functionals is provided in section 3.4. Detailed treatment of ground-state two-point functionals is in [15].

3.1. Thomas–Fermi noninteracting free-energy

The grand potential equation (2), evaluated for the noninteracting HEG of constant density n in volume V, gives the HEG noninteracting free-energy in terms of the Fermi–Dirac integrals $I_\alpha(\eta)$ [27, 29, 54]

$$\mathcal{F}_s^{\mathrm{HEG}}(n,T)=\Omega_s^{\mathrm{HEG}}(n)-\mu\left(\frac{\partial\Omega_s^{\mathrm{HEG}}(n)}{\partial\mu}\right)_{T,V}=V\frac{\sqrt{2}}{\pi^2\beta^{5/2}}\left[-\frac{2}{3}I_{3/2}(\beta\mu)+\beta\mu I_{1/2}(\beta\mu)\right], \tag{5}$$

where $\beta=(k_B\mathrm{T})^{-1}$. I_α is the FD integral [54]

$$I_\alpha(\eta):=\int_0^\infty \mathrm{d}x\frac{x^\alpha}{1+\exp(x-\eta)}\,,\quad \alpha>-1$$
$$I_{\alpha-1}(\eta)=\frac{1}{\alpha}\frac{\mathrm{d}}{\mathrm{d}\eta}I_\alpha(\eta)\,. \tag{6}$$

The chemical potential μ is determined from

$$n=-\frac{1}{V}\frac{\partial\Omega}{\partial\mu}\Big|_{\mathrm{T},V}=\frac{\sqrt{2}}{\pi^2\beta^{3/2}}I_{1/2}(\beta\mu)\,. \tag{7}$$

The LDA noninteracting free-energy, i.e. the finite-T TF density functional, is obtained by integrating the TF free-energy density corresponding to equation (5) with the local density substitution $n\to n(\mathbf{r})$:

$$\mathcal{F}_s^{\mathrm{TF}}[n]=\int f_s^{\mathrm{TF}}(n(\mathbf{r}),\mathrm{T})\,\mathrm{d}\mathbf{r}\,. \tag{8}$$

Here

$$f_s^{\mathrm{TF}}(n(\mathbf{r}),\mathrm{T})=\frac{\sqrt{2}}{\pi^2\beta^{5/2}}\left[-\frac{2}{3}I_{3/2}(\beta\mu)+\beta\mu I_{1/2}(\beta\mu)\right]_{n=n(\mathbf{r})}, \tag{9}$$

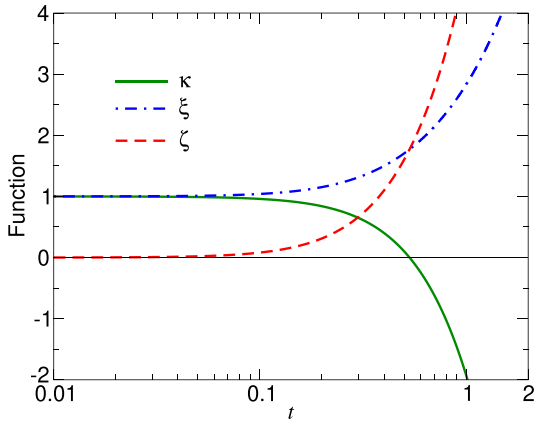

Figure 1. Behavior of functions $\kappa(t)$, $\xi(t)$ and $\zeta(t)$. Reprinted figure with permission from [29], Copyright (2012) by the American Physical Society.

and the local chemical potential μ is defined by $n(\mathbf{r})$ through equation (7). After some algebra, equation (9) takes the factorized form

$$f_{\rm s}^{\rm TF}(n,T) = \tau_0^{\rm TF}(n)\,\kappa(\beta\mu)\,, \tag{10}$$

with $\tau_0^{\rm TF}(n) = 0.3(3\pi^2)^{2/3}n^{5/3}$ and

$$\kappa(\beta\mu) = \frac{5}{2}\left(\frac{3}{2}I_{1/2}(\beta\mu)\right)^{-5/3}\left[-\frac{2}{3}I_{3/2}(\beta\mu) + \beta\mu I_{1/2}(\beta\mu)\right]. \tag{11}$$

In terms of the reduced temperature, $t = {\rm T}/{\rm T_F} = 2/\beta[3\pi^2 n]^{2/3}$ (with ${\rm T_F} = 2k_{\rm B}/[3\pi^2 n]^{2/3}$ the Fermi temperature), equation (7) can be transformed to

$$I_{1/2}(\beta\mu) = \frac{n\pi^2\beta^{3/2}}{\sqrt{2}} = \frac{2}{3t^{3/2}}\,. \tag{12}$$

Given that $I_{1/2}(\beta\mu)$ is a strictly increasing function as $(\beta\mu)$ increases and taking into account that $I_{1/2}(\beta\mu)$ is a function of t (equation (12)), we conclude that $(\beta\mu)$ is a function of t also. Hence $\kappa(\beta\mu)$ in equation (11) is a function of t as well (further details are in [29]). The noninteracting entropic and kinetic energy densities can be found from equation (10) by invoking the standard thermodynamic relations $\sigma_{\rm s}^{\rm TF}(n,t) = -\partial f_{\rm s}^{\rm TF}/\partial {\rm T}|_n = \tau_0^{\rm TF}(n)\zeta(t)$ and where the kinetic and entropic t-dependent dimensionless factors ξ and ζ are related by the standard thermodynamic relation leading to the following relations between t dependent functions, $\xi(t) = \kappa(t) - t\partial\kappa(t)/\partial t$ and $\zeta(t) = -t\partial\kappa(t)/\partial t$.

Figure 1 shows κ, ξ, and ζ as functions of the reduced temperature. The kinetic energy t-dependent factor ξ reduces to unity in the zero-T limit, hence the finite-T Thomas–Fermi kinetic energy reduces properly to the ground-state TF kinetic energy density $\tau_0^{\rm TF}(n)$. As expected, the entropic ζ factor vanishes in the zero-T limit. Both ξ and ζ functions are non-negative, so both the kinetic and entropic terms are non-negative. The noninteracting free-energy function κ becomes negative at $t \approx 0.54$ when the entropic term becomes dominant.

3.2. Second-order gradient expansion and GGA framework

The second-order gradient correction to the Thomas–Fermi functional equation (10), developed by Perrot [28], takes the form of the zero-T correction scaled by a function of the reduced temperature

$$f_{\rm s}^{(2)}(n,\nabla n,{\rm T}) = \tau_0^{\rm TF}(n)\,\frac{5}{27}s^2\widetilde{B}(t)\,, \tag{13}$$

where

$$s := |\nabla n|/2\left(3\pi^2\right)^{1/3}n^{4/3} \tag{14}$$

is the dimensionless reduced density gradient that is used as a variable in both ground-state GGA noninteracting kinetic energy functionals and XC functionals. The dimensionless function $\widetilde{B}$ is a combination of Fermi–Dirac integrals (also see [54]). As such $\widetilde{B}$ is a function of $\beta\mu$ or a function of t:

$$\widetilde{B}(t) = -3\frac{I_{1/2}(\beta\mu) I_{-3/2}(\beta\mu)}{I^2_{-1/2}(\beta\mu)}. \tag{15}$$

The result is the second-order gradient expansion (or second-order gradient approximation)

$$f_{\rm s}^{\rm GE2}(n, \nabla n, {\rm T}) = \tau_0^{\rm TF}(n)\,\kappa(t)\left(1 + \frac{5}{27}s^2\widetilde{B}(t)/\kappa(t)\right), \tag{16}$$

Equation (16) can be rendered in the usual GGA form, namely as the LDA energy density times an enhancement factor which is a function of another dimensionless variable

$$f_{\rm s}^{\rm GE2}(n, \nabla n, {\rm T}) = f_{\rm s}^{\rm TF}(n, {\rm T})\,F_{\rm f}(s_{\rm f}) \tag{17}$$

with

$$s_{\rm f} := s^2\widetilde{B}(t)/\kappa(t) \tag{18}$$

being the temperature dependent noninteracting free-energy reduced density gradient. As is evident from figure 1, $s_{\rm f}$ defined in this way has a pole when $\kappa(t)$ crosses zero. This bit of analysis led to construction of the finite-T GGA framework in [29], with the kinetic and entropic contributions treated separately, to wit

$$\sigma_{\rm s}^{\rm GE2}(n, \nabla n, {\rm T}) = -\frac{\partial f_{\rm s}^{\rm GE2}(n, \nabla n, {\rm T})}{\partial {\rm T}}\Big|_n = \frac{1}{\rm T}\tau_0^{\rm TF}(n)\,\zeta(t)\left(1 - \frac{5}{27}s^2\frac{t}{\zeta(t)}\frac{{\rm d}\widetilde{B}(t)}{{\rm d}t}\right). \tag{19}$$

With $\tau_{\rm s}^{\rm GE2} = f_{\rm s}^{\rm GE2} + {\rm T}\sigma_{\rm s}^{\rm GE2}$, one then has

$$\tau_{\rm s}^{\rm GE2}(n, \nabla n, {\rm T}) = \tau_0^{\rm TF}(n)\,\xi(t) \times \left(1 + \frac{5}{27}s^2\frac{1}{\xi(t)}\left[\widetilde{B}(t) - t\frac{{\rm d}\widetilde{B}(t)}{{\rm d}t}\right]\right). \tag{20}$$

Then by defining the kinetic and entropic T-dependent reduced density gradients as

$$\begin{aligned} s_\tau(n, \nabla n, {\rm T}) &= s(n, \nabla n)\sqrt{\frac{\widetilde{B}(t) - t{\rm d}\widetilde{B}(t)/{\rm d}t}{\xi(t)}}, \\ s_\sigma(n, \nabla n, {\rm T}) &= s(n, \nabla n)\sqrt{\frac{t{\rm d}\widetilde{B}(t)/{\rm d}t}{\zeta(t)}}, \end{aligned} \tag{21}$$

one has the noninteracting free-energy composed of generalizations of the SGA kinetic and entropic contributions equations (19)–(20)

$$\begin{aligned} \mathcal{F}_{\rm s}^{\rm GGA}[n] = &\int \tau_0^{\rm TF}(n)\,\xi(t)\,F_\tau(s_\tau)\,{\rm d}\mathbf{r}. \\ &- \int \tau_0^{\rm TF}(n)\,\zeta(t)\,F_\sigma(s_\sigma)\,{\rm d}\mathbf{r}. \end{aligned} \tag{22}$$

In these expressions, F_τ and F_σ are the noninteracting kinetic energy and entropic enhancement factors dependent on the reduced density gradients s_τ and s_σ respectively. The two enhancement factors are not independent. In the GE2 case, $F_\tau^{\rm GE2}(s_\tau) = (1 + \frac{5}{27}s_\tau^2)$, $F_\sigma^{\rm GE2}(s_\sigma) = (1 - \frac{5}{27}s_\sigma^2)$, thus the two factors have the simple relationship

$$F_\sigma^{\rm GE2}(x) = 2 - F_\tau^{\rm GE2}(x). \tag{23}$$

In fact, equation (23) is an accurate approximation in the general case [29], so that for a specified $F_\tau(s_\tau)$, the entropic enhancement factor is

$$F_\sigma(s_\sigma) \approx 2 - F_\tau(s_\sigma). \tag{24}$$

A consequence of this approximation is that the two terms in equation (22) do not preserve a strict interpretation as the kinetic and entropic contributions. However, the difficulty is resolved by invocation of the standard thermodynamic relation, such that the two contributions are given by

$$\begin{aligned}\mathcal{S}_{\rm s}^{\rm GGA} &= -\frac{\partial \mathcal{F}_{\rm s}^{\rm GGA}}{\partial \mathrm{T}}\Big|_{N,V}\\ \mathcal{T}_{\rm s}^{\rm GGA} &= \mathcal{F}_{\rm s}^{\rm GGA} + \mathrm{T}\mathcal{S}_{\rm s}^{\rm GGA}.\end{aligned} \tag{25}$$

Equations (15), (21), (22), (24) and (25) define the framework for constructing noninteracting free-energy density functionals at the GGA level of refinement that was developed in [29]. By use of that procedure, virtually any ground-state GGA noninteracting kinetic energy functional can be extended to finite T. Three steps are required, (i) select a ground-state functional with its kinetic energy enhancement factor given by $F_t(s)$; (ii) construct the finite-T kinetic energy enhancement factor as $F_\tau(s_\tau) \equiv F_t(s_\tau)$; (iii) construct the entropic enhancement factor as $F_\sigma(s_\sigma) \equiv 2 - F_\tau(s_\sigma)$.

In addition to the functionals presented in [29], there are two successful examples of construction of noninteracting free-energy functionals obtained from the constraint-based ground-state kinetic energy via the foregoing procedure. One is VT84F. It is constrained to satisfy various positivity conditions on the so-called Pauli potential, including for densities that have a proper Kato cusp [55]. Its form is

$$F_\tau^{\rm VT84F}(s_\tau) = 1 - \frac{\mu s_\tau^2 \mathrm{e}^{-\alpha s_\tau^2}}{1+\mu s_\tau^2} + \left(1 - \mathrm{e}^{-\alpha s_\tau^{m/2}}\right)\left(s_\tau^{-n/2} - 1\right) + \frac{5}{3}s_\tau^2, \tag{26}$$

with $m = 8$, $n = 4$, $\mu = 2.778$ and $\alpha = \mu - 5/3 + 5/27$. The other is LKT [32], specifically adapted to use with local pseudopotentials. It has the very simple enhancement factor

$$F_\tau^{\rm LKT}(s_\tau) = \frac{5}{3}s_\tau^2 + \frac{1}{\cosh(as_\tau)}, \tag{27}$$

with $a = 1.3$.

3.3. Fourth-order gradient expansion and meta-GGA functionals

The fourth-order gradient expansion (GE4) for the noninteracting free-energy density of a weakly inhomogeneous electron density at any T, $f_{\rm s}^{\rm GE4}(n, \nabla n, \nabla^2 n, \mathrm{T}) = f_{\rm s}^{\rm GE2}(n, \nabla n, \mathrm{T}) + f_{\rm s}^{(4)}(n, \nabla n, \nabla^2 n, \mathrm{T})$, was derived by Geldart and Sommer [56, 57], and Bartel *et al* [54]. The Laplacian-dependent fourth-order correction is

$$f_{\rm s}^{(4)}\left(n, \nabla n, \nabla^2 n, \mathrm{T}\right) = \tau_0^{\rm TF}(n)\left[\frac{8}{81}q^2\widetilde{C} - \frac{1}{9}s^2 q\widetilde{D} + \frac{8}{243}s^4\widetilde{E}\right]. \tag{28}$$

In it, the dimensionless reduced density Laplacian is given by

$$q := \nabla^2 n / 4\left(3\pi^2\right)^{2/3} n^{5/3}. \tag{29}$$

(Remark: In a few of the orbital-free KE papers what is denoted here as q was denoted as p. But in most of the DFT literature, $p := s^2$ and q is as in equation (29), so we have used those definitions here.) As in the GE2 case, $\widetilde{C}$, $\widetilde{D}$, and $\widetilde{E}$ are combinations of Fermi–Dirac η-dependent integrals, making them functions of the reduced temperature t

$$\widetilde{C}(\eta) = \frac{5\times 3^{11/3}}{2^{11/3}} I_{1/2}^{5/3}(\eta)\left[\frac{1}{9}\frac{I_{-3/2}^2(\eta)}{I_{-1/2}^3(\eta)} - \frac{1}{5}\frac{I_{-5/2}(\eta)}{I_{-1/2}^2(\eta)}\right], \tag{30}$$

$$\widetilde{D}(\eta) = \frac{5\times 2^{1/3}}{3^{1/3}} I_{1/2}^{8/3}(\eta)\left[-3\frac{I_{-7/2}(\eta)}{I_{-1/2}^3(\eta)} + \frac{33}{10}\frac{I_{-3/2}(\eta)I_{-5/2}(\eta)}{I_{-1/2}^4(\eta)} - \frac{I_{-3/2}^3(\eta)}{I_{-1/2}^5(\eta)}\right], \tag{31}$$

and

$$\begin{aligned}\widetilde{E}(\eta) = \frac{5\times 3^{14/3}}{2^{2/3}} I_{1/2}^{11/3}(\eta)\Bigg[&-\frac{7}{96}\frac{I_{-9/2}(\eta)}{I_{-1/2}^4(\eta)} - \frac{1}{15}\frac{I_{-3/2}^2(\eta)I_{-5/2}(\eta)}{I_{-1/2}^6(\eta)} + \frac{1}{72}\frac{I_{-3/2}^4(\eta)}{I_{-1/2}^7(\eta)}\\ &+\frac{1}{12}\frac{I_{-3/2}(\eta)I_{-7/2}(\eta)}{I_{-1/2}^5(\eta)} + \frac{1}{32}\frac{I_{-5/2}^2(\eta)}{I_{-1/2}^5(\eta)}\Bigg],\end{aligned} \tag{32}$$

where $\eta = \beta\mu$. In parallel with equations (19)–(22), by invoking the standard thermodynamic relation, the fourth-order entropic and kinetic terms are defined as [34]

$$\sigma_{\rm s}^{(4)}\left(n,\nabla n,\nabla^2 n,{\rm T}\right) = \frac{1}{\rm T}\tau_0^{\rm TF}(n)\,\zeta(t)\times\left[-\frac{8}{81}q^2 c_\sigma(t)+\frac{1}{9}s^2 q d_\sigma(t)-\frac{8}{243}s^4 e_\sigma(t)\right], \tag{33}$$

and

$$\tau_{\rm s}^{(4)}\left(n,\nabla n,\nabla^2 n,{\rm T}\right) = \tau_0^{\rm TF}(n)\,\xi(t)\times\left[\frac{8}{81}q^2 c_\tau(t)-\frac{1}{9}s^2 q d_\tau(t)+\frac{8}{243}s^4 e_\tau(t)\right]. \tag{34}$$

Two sets of t-dependent functions in equations (33) and (34) involve derivatives of the functions $\widetilde{C}$, $\widetilde{D}$, and $\widetilde{E}$, and define temperature dependences of the fourth-order gradient term

$$\begin{aligned} c_\sigma(t) &= \frac{t}{\zeta(t)}\frac{{\rm d}\widetilde{C}(t)}{{\rm d}t},\\ d_\sigma(t) &= \frac{t}{\zeta(t)}\frac{{\rm d}\widetilde{D}(t)}{{\rm d}t},\\ e_\sigma(t) &= \frac{t}{\zeta(t)}\frac{{\rm d}\widetilde{E}(t)}{{\rm d}t}, \end{aligned} \tag{35}$$

and

$$\begin{aligned} c_\tau(t) &= \frac{1}{\xi(t)}\left[\widetilde{C}(t)-t\frac{{\rm d}\widetilde{C}(t)}{{\rm d}t}\right],\\ d_\tau(t) &= \frac{1}{\xi(t)}\left[\widetilde{D}(t)-t\frac{{\rm d}\widetilde{D}(t)}{{\rm d}t}\right],\\ e_\tau(t) &= \frac{1}{\xi(t)}\left[\widetilde{E}(t)-t\frac{{\rm d}\widetilde{E}(t)}{{\rm d}t}\right], \end{aligned} \tag{36}$$

for the entropy and kinetic energy densities respectively.

The ground-state noninteracting kinetic energy meta-GGA enhancement factor $F_{\rm s}^{\rm MGGA-GSA}(s,q)$ depends on the dimensionless reduced density gradient and Laplacian variables, s, equation (14), and q, equation (29). The meta-GGA noninteracting free-energy functional, by analogy with equation (22), has the kinetic and entropic terms with respective second- and fourth-order temperature dependencies incorporated via dimensionless variables equations (21), (35) and (36)

$$\begin{aligned} &\mathcal{F}_{\rm s}^{\rm MGGA}[n] = \mathcal{T}_{\rm s}^{\rm MGGA}[n]-{\rm T}\mathcal{S}_{\rm s}^{\rm MGGA}[n]\equiv\\ &\int \tau_0^{\rm TF}(n)\,\xi(t)\,F_\tau(s,q,\{b_\tau,c_\tau,{\rm d}_\tau,e_\tau\})\,{\rm d}\mathbf{r}-\\ &\int \tau_0^{\rm TF}(n)\,\zeta(t)\,F_\sigma(s,q,\{b_\sigma,c_\sigma,{\rm d}_\sigma,e_\sigma\})\,{\rm d}\mathbf{r}, \end{aligned} \tag{37}$$

where the second-order kinetic and entropic temperature dependent functions $b_\tau(t) = [\widetilde{B}(t) - t\widetilde{B}'(t)]/\xi(t)$ and $b_\sigma(t) = t\widetilde{B}'(t)/\zeta(t)$ are introduced such that s_τ and s_σ equation (21) can be represented as $s_\tau(n,\nabla n,{\rm T}) = s(n,\nabla n)\sqrt{b_\tau(t)}$ and.

The kinetic and entropic enhancement factors in equation (37) are related as

$$F_\sigma(s,p,\{b_\sigma,c_\sigma,d_\sigma,e_\sigma\}) \approx 2 - F_\tau(s,p,\{b_\sigma,c_\sigma,d_\sigma,e_\sigma\}). \tag{38}$$

Equations (37) and (38) represent generalizations of the finite-T GE4 which can be presented in the form of equation (37) with the kinetic and entropic enhancement factors defined by

$$F_\tau^{\rm GE4}(s,q,\{b_\tau,c_\tau,d_\tau,e_\tau\}) = 1+\frac{5}{27}s^2 b_\tau(t)+\left[\frac{8}{81}q^2 c_\tau(t)-\frac{1}{9}s^2 q d_\tau(t)+\frac{8}{243}s^4 e_\tau(t)\right], \tag{39}$$

and

$$F_\sigma^{\rm GE4}(s,q,\{b_\sigma,c_\sigma,d_\sigma,e_\sigma\}) = 2 - F_\tau^{\rm GE4}(s,q,\{b_\sigma,c_\sigma,d_\sigma,e_\sigma\}), \tag{40}$$

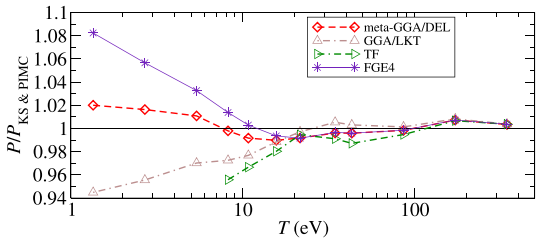

Figure 2. Comparison of performance of four noninteracting free energy functionals. Shown is the pressure for D at $\rho = 3.11814$ g cm^{-3} relative to the pressure from the combined conventional KS (T $\leqslant$ 86 eV) and PIMC (T $>$ 86 eV) values [58]. Both OF-DFT and conventional KS calculations used the KDT16 GGA [36] XC free energy.

(compare to a sum of the GE2, and the individual fourth-order term, defined by equations (19)–(20) and (33)–(34)). The approximate relation equation (38) is, as in the GGA case equation (24), implied by the fourth-order gradient expansion (see further details in [34]). The kinetic and entropic contributions can be calculated from equation (25) with use of the $\mathcal{F}_{\rm s}^{\rm MGGA}[n]$ functional.

Within the foregoing framework, a density-Laplacian-level noninteracting free-energy functional was reported in [34]. The double exponent Laplacian-dependent functional (DEL) is defined by the kinetic energy enhancement factor

$$F_{\tau}^{\rm DEL}(s,q,\{a_{\tau},..,e_{\tau}\}) = \frac{5}{3}s^2 b_{\tau} + \frac{1}{2}\left\{e^{-2\mu s^2 b_{\tau}} + e^{-2\mu^2 s^4 b_{\tau}^2 + 2\nu s^4 e_{\tau}}\right\} + \alpha q^2 c_{\tau} - \beta s^2 q d_{\tau}\,, \tag{41}$$

with $\mu = 40/27$, $\nu = 8/243$, $\alpha = 8/81$, $\beta = 1/9$, and the entropic enhancement factor defined by equation (38). One of the important constraints that the DEL functional satisfies is that it reduces to the fourth-order gradient expansion equations (16) and (28) in the slowly-varying density limit.

Figure 2 compares the behavior of the LDA, GGA, and meta-GGA rungs of the Perdew–Schmidt ladder by showing AIMD results from the TF, LKT, GE4, and DEL noninteracting free-energy functionals for dense deuterium at material density $\rho_{\rm D} = 3.118\,14$ g cm^{-3} ($r_{\rm s} = 1.20$ bohr) in the temperature range between 1.35 and 345 eV. We followed reference [34] for these AIMD simulations.The relative pressure is calculated with respect to combined conventional KS and PIMC reference data [58]. Both the orbital-free and conventional KS simulations were performed in combination with the KDT16 GGA free energy XC functional (see section 4.2) to provide compatibility with the PIMC data. The simplest TF approximation has the largest error at T below $\approx$ 20 eV. (Remark: The TF simulations did not converge for T$<$ 8 eV.) The LKT GGA-level functional has relative error close to 6% at T = 1.34 eV. That decreases to about 2% or less for T above 10 eV. The finite-T fourth-order gradient expansion provides poorer low-T results compared to the LKT GGA. The relative error at the lowest T exceeds 8% and goes down to the level of 2% and below at T $\geqslant$ 8.21 eV. The meta-GGA level DEL functional provides the most accurate results with relative error not exceeding 2%. This comparison illustrates the improvement of accuracy expected to accompany the introduction of more ingredient functional variables in constraint-based density functionals.

3.4. Non-local noninteracting free-energy functionals

The non-local (two-point) noninteracting free-energy functional developed in [31] has the form

$$\mathcal{F}_{\rm s,2}[n] =_{\beta} T_{\rm vW}[n] + \mathcal{F}_{\rm TF}[n] + \int \mathbf{dr}\mathbf{dr}'\, n^a(\mathbf{r})\, w(|\mathbf{r}-\mathbf{r}'|)\, n^b(\mathbf{r}') \tag{42}$$

with $a = b = 5/6$. It has a novel modified von Weizsäcker term

$${}_{\beta}T_{\rm vW}[n] := \int \mathbf{dr}\mathbf{dr}'\{(\nabla n(\mathbf{r}))^{1/2}\cdot(\nabla n(\mathbf{r}'))^{1/2}\}\{\delta(\mathbf{r}-\mathbf{r}') + \beta(|\mathbf{r}-\mathbf{r}'|)\}\,. \tag{43}$$

The functional equation (43) is constrained to reproduce the exact density response of the HEG at finite-T, a requirement which yields a relation between the w and β kernels. This results in the T-dependent Wang-Teter-like [59] kernel. A prior version of this functional was developed in [60].

Quite recently Ma *et al* [33] presented a line-integral derivation of a counterpart two-point noninteracting free-energy functional that, in principle, is more general. It has the form of equation (43) without the modification to the von Weizsäcker term and with the non-local contribution

$$\mathcal{F}_{\rm s,2}^{\rm XWMF}[n] = \int \mathbf{dr}\mathbf{dr}'\, n^{\kappa+\frac{5}{6}}(\mathbf{r})\,\omega_1(\mathbf{r},\mathbf{r}')\, n^{\kappa+\frac{5}{6}}(\mathbf{r}') + \int \mathbf{dr}\mathbf{dr}'\, n^{\kappa+\frac{11}{6}}(\mathbf{r})\,\omega_2(\mathbf{r},\mathbf{r}')\, n^{\kappa+\frac{5}{6}}(\mathbf{r}')\,. \tag{44}$$

The expression combines the zeroth-order term (that reduces to the Wang-Teter non-local term for the HEG) and first-order term (that accounts for the density inhomogeneity) of the Taylor expansion of the density-dependent function G that arises in the second derivative of the non-local free-energy for the inhomogeneous electron gas along the line-integral path (see details in [33]).

This non-local functional works very well for (semi-)conducting systems such as warm dense hydrogen/deuterium and liquid Al. So far the functional has been applied only to those two systems. Comparison between the finite-T semilocal and this non-local functional for warm dense deuterium demonstrated that the one-point meta-GGA/DEL equations (37)–(41) and the two-point non-local functionals have very similar performance. The relative total pressure error of the two with respect to the reference data for deuterium along the 4.048 g cm^{-3} isochore never exceeds 2%. However, the transferability of such two-point functionals to semiconductors and insulators is poor [23, 61] because of the strict adherence to the HEG response. That is suitable only for systems with weakly inhomogeneous electron densities.

The non-local XWMF noninteracting free-energy functional (with the two-point non-local part defined by equation (44)) was applied to static lattice calculations of Al and Si with employment of valence-only LPPs, and to AIMD simulations of warm dense H, He, and H-He mixtures (for two densities, 10 and 160 g cm^{-3}). Some of those results were compared to results from the one-point LKTF GGA noninteracting free-energy functional. Figure 1 in [33] suggests that except for Al at relatively low T, LKTF is fully competitive with XWMF. Furthermore, table 1 in the same reference shows that the one-point LKTF GGA is almost as good as the non-local XWMF on dense hydrogen.

With AE LPPs, so far the XWMF non-local functional has been applied only to H (in the range of material densities between 0.6 and 8 g cm^{-3}), and to H, He, and H–He mixtures at relatively high material densities, 10 and 160 g cm^{-3}. In that regime, all these systems are expected to be metallic with relatively smooth electron density. Though the XWMF kernel is based on the first-order Taylor expansion that takes density inhomogeneity into account to some extent, its performance for highly inhomogeneous systems such as He at material densities below 1 g cm^{-3} and/or LiD with AE LPPs (see examples in [34]) is unknown yet.

4. XC orbital-free free-energy functionals

In this section we provide a brief description of recent progress in development of non-empirical XC free-energy density functionals at the LDA, GGA, and meta-GGA levels of complexity. Such XC functionals are required *both* for conventional KS-DFT and OF-DFT simulations of matter under extreme conditions. Development of XC free-energy functionals essentially follows the finite-T analog of the Perdew–Schmidt ladder [53] with the first two rungs (LDA and GGA) fully developed in [35] (with modest refinements using the same approach in [38]) and [36] respectively.

For both T$=0$ and T>0, the third, or meta-GGA rung of the Perdew–Schmidt ladder has two versions, orbital-dependent and orbital-independent. The orbital-dependent form is dominant in ground-state development and applications, hence is obviously problematic for OF-DFT. The orbital-independent forms typically depend on n, the reduced density gradient s defined at equation (14), and the reduced density Laplacian q defined at equation (29). We return to this distinction in more detail below. For perspective, here it suffices to say that meta-GGA free-energy XC functionals have been developed in a straightforward, orbital-dependent way [62], as well as an orbital-free version as a universal additive thermal correction using a perturbation-like approach [40]. The second rung is represented by the fully-thermal KDT16 GGA with temperature dependent reduced density gradients, and by two rather more approximate schemes that take thermal XC effects into account at the LDA level via additive [37] or multiplicative [63] corrections to the ground-state PBE XC expression.

4.1. LDA

The first accurate analytical representation for the XC free energy of the HEG was the Karasiev–Sjostrom–Dufty–Trickey (KSDT) parametrization [35] of restricted path integral Monte Carlo (RPIMC) data for the HEG at finite temperature [64] and the T $=0$ K data of [65]. The KSDT parametrization constitutes the local spin density approximation for the XC free-energy. The corrected KSDT representation (corrKSDT), based on improved quantum Monte Carlo (QMC) data [66], was published in [36]. The essentially equivalent representation (with slight differences in MC data and analysis detail) was published in [38]. The equivalence of the two as well as limitations of the representation (see below also) are discussed in [41].

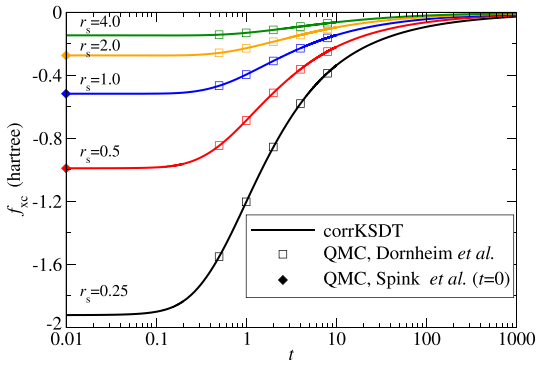

Figure 3. Comparison between f_{xc} values from the corrKSDT parametrization and QMC data from [66] for the unpolarized HEG at $r_s = 0.25$, 0.5, 1, 2, and 4. The ground-state limit ($t = 0$, [65]) QMC values also are shown. Reprinted figure with permission from [41], Copyright (2019) by the American Physical Society.

The KSDT XC free-energy per particle, for the spin-unpolarized case, has the form of a [2,2] Padé approximant [67] in the $r_s^{1/2}$ variable ($r_s = (3/4\pi n)^{1/3}$) with t-dependent coefficients

$$f_{xc}^{LDA}(r_s,t) = -\frac{1}{r_s}\frac{a(t) + b(t)\, r_s^{1/2} + c(t)\, r_s}{1 + d(t)\, r_s^{1/2} + e(t)\, r_s}. \tag{45}$$

The XC internal energy per particle is evaluated via the standard thermodynamic relation (analogous with equation (25)) for XC

$$\varepsilon_{xc}^{LDA}(r_s,t) = f_{xc}^{LDA}(r_s,t) - t\frac{\partial f_{xc}^{LDA}(r_s,t)}{\partial t}\bigg|_{r_s}. \tag{46}$$

The X free-energy per particle LDA has the factorized form [28]

$$f_x^{LDA}(n,t) = \varepsilon_x^{LDA}(n)\,\widetilde{A}_x(t)\,, \tag{47}$$

$$\widetilde{A}_x(t) = \frac{t^2}{2}\int_{-\infty}^{(\beta\mu)} I_{-1/2}^2(\eta)\,\mathrm{d}\eta\,. \tag{48}$$

With the help of equations (45) and (47), the LDA correlation free-energy per particle is defined as

$$f_c^{LDA}(n,t) = f_{xc}^{LDA}(n,t) - f_x^{LDA}(n,t)\,. \tag{49}$$

(Remarks: The r_s and n dependencies can be used interchangeably. Also the t-dependence implicates both n and T dependencies.)

In addition to demonstrating that the corrKSDT parametrization matches the available finite-T and T= 0 K data essentially perfectly, figure 3 also shows how the XC free-energy magnitude decreases with increasing temperature for all r_s. For example, it drops approximately twofold at $t = 2$ for $r_s = 0.5$ as compared to the T= 0 K value, namely decreasing from $|-0.990|$ to $|-0.512|$ hartree. That highlights the importance of finite-T XC approximations for simulations at elevated temperature. It also is important to notice that the XC free-energy remains almost flat for values of t up to a few tenths of the Fermi temperature. In terms of the actual temperature T, a value of $t = 0.2$ for example, corresponds to T≈ 7.3, 29, 116, 465, and 1860 kK for $r_s = 4$, 2, 1, 0.5, and 0.25 respectively.

A detailed study of the significance of going beyond the ground-state approximation for XC appeared recently [68]. The focus system was warm dense hydrogen. Those authors had new PIMC data available for both H and H_2 as benchmarks. A direct comparison of free-energy LDA (GDSMFB in this case, but recalling the above discussion about equivalence), LDA, and PBE (both in the ground-state approximation) results with their PIMC data is not a facile way to detect the differences. A much clearer analysis emerges from use of their definition of a generalized reduced density gradient:

$$S(\alpha) := \frac{1}{N_e}\int \mathrm{d}n\, s[n]\left(\frac{n}{n_0}\right)^{\alpha}. \tag{50}$$

In it, s is as defined at equation (14) and n_0 is the average density. Examination of $S(\alpha)$ shows very clearly that free-energy LDA outperforms all of the ground-state GGA functionals they examined. Perhaps more

remarkably, free-energy LDA provides $S(\alpha)$ results of similar quality to those of the meta-GGA SCAN [69] used in the ground-state approximation.

This behavior of SCAN can be rationalized by recognizing that one of its key ingredients is the KS kinetic energy density τ_s. It is dependent on the orbitals and Fermi–Dirac occupations,

$$\tau_s := \tfrac{1}{2}\sum_i f_i |\nabla\varphi_i|^2 \,. \tag{51}$$

Usually it is assumed, implicitly, that the only thermal information in the ground-state approximation is provided by $n(\mathbf{r},\mathrm{T})$. But when SCAN is used as an approximation to $\mathcal{F}_{\mathrm{xc}}$, i.e. the ground-state approximation, the T-dependence in the Fermi–Dirac occupations introduces thermal information beyond that supplied by $n(\mathbf{r},\mathrm{T})$. It is quite plausible that the portion of the XC free energy taken into account thereby is greater than for a ground-state approximation by an E_{xc} that does not depend upon τ_s. See further discussion at the end of section 4.3.

Other important aspects of the corrKSDT (and GDSFMB [38, 39]) parametrization are discussed in [41]. In particular, we point out that the HEG specific heat,

$$c_v(r_s,t) = \frac{-1}{\mathrm{T_F}}\frac{\partial^2 f(r_s,t)}{\partial t^2}\bigg|_{r_s} \tag{52}$$

displays increasingly large and unphysical oscillations as r_s increases. Those are a consequence of the delicate balance between the parametrized X and C contributions. To our knowledge, no progress has been made to date on a revised parametrization with a more physically reliable second thermodynamic derivative.

4.2. GGA: fully thermalized and LDA-level corrected

The strategy for development of the GGA XC free-energy is similar to the development of the GGA noninteracting free-energy framework given in section 3.2: analyze the second-order finite-T gradient expansion for XC, define dimensionless reduced density variables with explicit temperature dependence for X and C, and construct a functional in the usual GGA spirit. Thus, to preserve proper density scaling, the GGA X and C are given by the LDA X and C free-energy densities multiplied by a function (enhancement factor) of X and C t-dependent variables. Obviously, those enhancement factors must reduce to accurate representations at zero-T of some well-tested zero-T counterpart so that the finite-T GGA XC will be accurate across the entire temperature regime.

The second-order gradient correction to the XC free-energy is the central ingredient for the development of the thermal GGA. It resembles the ground-state gradient coefficient, but with a T- and n-dependent coefficient [1, 70–73]

$$f_{\mathrm{xc}}^{(2)}(n,\nabla n,\mathrm{T}) = \tfrac{1}{2}g_{\mathrm{xc}}^{(2)}(n,\mathrm{T})\frac{|\nabla n(\mathbf{r})|^2}{n}\,. \tag{53}$$

Equation (53) can be partitioned into X and C contributions in the form

$$f_{\mathrm{xc}}^{(2)}(n,\nabla n,\mathrm{T}) = C_{\mathrm{x}}^{(2)}\varepsilon_{\mathrm{x}}^{\mathrm{LDA}}(n)s^2(n,\nabla n)\widetilde{B}_{\mathrm{x}}(t) + C_{\mathrm{c}}^{(2)}n^{1/3}s^2(n,\nabla n)\widetilde{B}_{\mathrm{c}}(n,t)\,, \tag{54}$$

where $\widetilde{B}_{\mathrm{x}}$ is a combination of Fermi–Dirac integrals. The gradient correction coefficient was evaluated numerically in [37] with use of a relation to the static local field correction [74, 75] and QMC data for the finite-T HEG [64]. The second-order gradient expansion for the X free energy, $f_{\mathrm{x}}^{\mathrm{GE2}} = f_{\mathrm{x}}^{\mathrm{LDA}} + f_{\mathrm{x}}^{(2)}$ can be written as [1, 70–73]

$$f_{\mathrm{x}}^{\mathrm{GE2}}(n,\nabla n,\mathrm{T}) = f_{\mathrm{x}}^{\mathrm{LDA}}(n,\mathrm{T})\left(1+\frac{8}{81}\frac{\widetilde{B}_{\mathrm{x}}(t)}{\widetilde{A}_{\mathrm{x}}(t)}s^2(n,\nabla n)\right)\,. \tag{55}$$

Equation (55) enables the definition of the appropriate dimensionless reduced density gradient variable with explicit T-dependence for the X free energy as

$$s_{2\mathrm{x}}(n,\nabla n,\mathrm{T}) \equiv s^2(n,\nabla n)\frac{\widetilde{B}_{\mathrm{x}}(t)}{\widetilde{A}_{\mathrm{x}}(t)}\,. \tag{56}$$

Additionally, numerically evaluated $g_{\mathrm{xc}}^{(2)}$ data in combination with equation (54) allow numerical evaluation of the function $\widetilde{B}_{\mathrm{c}}(n,t)$. Accurate analytic fits for the functions $\widetilde{A}_{\mathrm{x}}(t)$, $\widetilde{B}_{\mathrm{x}}(t)$, and $\widetilde{B}_{\mathrm{c}}(n,t)$ with properly incorporated asymptotic behavior were presented in [36, 76].

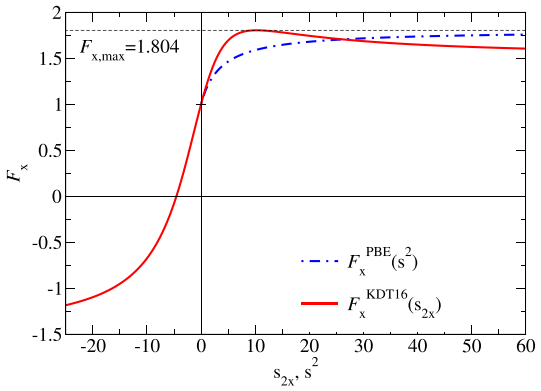

Figure 4. Comparison of the PBE and KDT16 exchange enhancement factors.

The correlation term in equation (54) is proportional to $\mathcal{Q}^2\widetilde{B}_c(r_s,t)$ with $\mathcal{Q}(n,\nabla n)=|\nabla n|/2k_s n$ the ground-state reduced density gradient for correlation and $k_s=2(3n/\pi)^{1/6}$ the Thomas–Fermi screening wave number. (Remark: To avoid notational overload, what is denoted here as $\mathcal{Q}$ is t in the original PBE paper [77] and denoted q in the KDT16 paper [36].) This motivated definition of the T-dependent reduced density gradient for correlation

$$\mathcal{Q}_c(n,\nabla n,T)=\mathcal{Q}(n,\nabla n)\sqrt{\widetilde{B}_c(n,t)}. \tag{57}$$

The fully thermal GGA exchange and correlation functional then was formulated in the form

$$\mathcal{F}_x^{GGA}[n]=\int nf_x^{LDA}(n,t)F_x(s_{2x})\,\mathrm{d}\mathbf{r}, \tag{58}$$

and

$$\mathcal{F}_c^{GGA}[n]=\int nf_c^{GGA}(n,\nabla n,t)\,\mathrm{d}\mathbf{r}. \tag{59}$$

The exchange enhancement factor and correlation free-energy per particle for the spin unpolarized case, (spin polarization function $\zeta=0$) are defined as

$$F_x(s_{2x}):=1+\frac{\nu_x s_{2x}}{1+\alpha|s_{2x}|}, \tag{60}$$

with $\nu_x=0.21951$, $\alpha=\nu_x/(F_{x,max}-1)$, $F_{x,max}=1.804$, and

$$f_c^{GGA}(n,\nabla n,t)=f_c^{LDA}(n,t)+H\left(f_c^{LDA},\zeta=0,\mathcal{Q}_c\right). \tag{61}$$

In the last expression, the PBE correlation function H is as defined in [77]. The KDT16 XC functional defined by equations (58)–(61) reduces by construction (with a minor difference) to the ground-state PBE functional in the zero-T limit

$$\lim_{T\to 0}\mathcal{F}_{xc}^{KDT16}[n]\approx E_{xc}^{PBE}[n]. \tag{62}$$

Figure 4 compares the KDT16 and PBE exchange enhancement factors shown as functions of s^2 and s_{2x} variables respectively. Both exchange functionals satisfy the Lieb–Oxford bound enforced locally ($F_x\leqslant 1.804$). Moreover, equation (60) recovers the PBE enhancement factor in the zero-T limit, given that $s_{2x}\to s^2$. Notably, the thermal X enhancement factor crosses zero and becomes negative at $t\gtrsim 1$ (see figure 1 in [36]).

A few years before KDT16 was published, an interesting approximate GGA XC free energy was built via an additive thermal LDA XC correction to a ground-state GGA [37]. Again with respect to the ground-state PBE functional, the scheme takes the 'subtract and add' form

$$f_{xc}^{addPBE}(n,\nabla n,t)=\varepsilon_{xc}^{PBE}(n,\nabla n)-\varepsilon_{xc}^{LDA}(n)+f_{xc}^{LDA}(n,t), \tag{63}$$

where the PBE XC energy per particle is defined via the X enhancement factor $F_{\rm x}^{\rm PBE}$ and correlation function H as

$$\varepsilon_{\rm xc}^{\rm PBE}(n,\nabla n)=\varepsilon_{\rm x}^{\rm LDA}(n)F_{\rm x}^{\rm PBE}\left(s^2\right)+\varepsilon_{\rm c}^{\rm LDA}(n)+H\left(\varepsilon_{\rm x}^{\rm LDA},\mathcal{Q}\right). \tag{64}$$

In rather the same spirit, Kozlowski *et al* [63] recently produced a multiplicative rather than additive thermal correction. In it, the ground-state PBE XC is scaled by thermal corrections at the LDA level via a 'divide and multiply' approach. This yields what those authors call the locally thermal PBE ('ltPBE') approximation

$$f_{\rm xc}^{\rm ltPBE}(n,\nabla n,t)=\varepsilon_{\rm xc}^{\rm PBE}(n,\nabla n)\frac{f_{\rm xc}^{\rm LDA}(n,t)}{\varepsilon_{\rm xc}^{\rm LDA}(n)}\equiv\varepsilon_{\rm xc}^{\rm LDA}(n)F_{\rm xc}^{\rm ltPBE}(n,\nabla n,t), \tag{65}$$

where the second line in equation (65) defines an XC 'enhancement factor' introduced in [63]. It is a dimensionless function that depends on the ground-state X and C reduced density gradients (hidden in $\varepsilon_{\rm xc}^{\rm PBE}(n,\nabla n)$) and on t via the LDA XC free-energy density $f_{\rm xc}^{\rm LDA}$

$$F_{\rm xc}^{\rm ltPBE}(n,\nabla n,t)\equiv\frac{\varepsilon_{\rm xc}^{\rm PBE}(n,\nabla n)}{\varepsilon_{\rm xc}^{\rm LDA}(n)}\frac{f_{\rm xc}^{\rm LDA}(n,t)}{\varepsilon_{\rm xc}^{\rm LDA}(n)}. \tag{66}$$

The foregoing expressions are valid for the specific case of uniform spin-polarization ($\zeta=0$ or $\zeta=1$).

We emphasize that in both the additive equation (63) and multiplicative equation (65)–(66) schemes, there is an additional approximation beyond what is intrinsic to the GGA level of refinement. Both schemes account for thermal XC corrections at the LDA level only. The spatial inhomogeneity effects are described by the ground state PBE gradient-dependent functions without any explicit temperature dependence, namely through the functions $F_{\rm x}^{\rm PBE}(s^2)$ and $H(\varepsilon_{\rm x}^{\rm LDA},\mathcal{Q})$ with ground-state variables s and $\mathcal{Q}$ for exchange and correlation respectively; see equation (64). In general such schemes therefore miss the temperature dependences defined by the gradient expansion term equation (54) and thus do not reproduce the second-order finite-T gradient expansion in the limit of weakly varying density.

The KDT16 XC free-energy does reproduce T-dependences consistent with the gradient expansion. That is important especially in the WDM regime. There the temperature approaches neither the low-T nor high-T limit. It is to be expected that KDT16 is more accurate than either the addPBE or the ltPBE approximations for weakly inhomogeneous systems at such intermediate temperatures. Because all three functionals reduce to the same limits (ground-state PBE and the finite-T LDA for the low-T and high-T cases respectively), in both the low- and high-T limits all three functionals should converge to the same accuracy. Preliminary results show that for selected density-temperature conditions of dense deuterium, when the ltPBE relative pressure errors are around 2% (same magnitude as for the thermal LDA XC), the KDT16 relative errors are 1% or less. At least in that example, the ltPBE XC does not improve upon the thermal LDA XC, confirmation that the thermalization is done only at the LDA level of refinement.

4.3. Meta-generalized gradient XC approximations

Development of orbital-free meta-GGA XC functionals has taken such a different path from the noninteracting case that it is valuable to summarize the ground-state case first.

As mentioned at the outset of this section, even for the ground state, the meta-GGA rung of the Perdew–Schmidt refinement ladder has an ambiguity. Our earlier discussion (section 3.3) of the noninteracting contribution might lead one to expect the meta-GGA rung of XC functionals to involve introduction of $\nabla^2 n$ dependence through the dimensionless variable q defined at equation (29). But historically, the development of ground-state meta-GGA XC functionals, which preceded the noninteracting meta-GGA development, took a different route. Instead of q dependence, ground state meta-GGA XC development almost exclusively exploits the information in the orbital-dependent KS kinetic energy density $\tau_{\rm s}$ equation (51).

Most, but not all, ground-state meta-GGA XC DFAs use the 'iso-orbital indicator'

$$\alpha(\mathbf{r}):=\frac{\tau_{\rm s}-\tau_{\rm vW}}{\tau_0^{\rm TF}} \tag{67}$$

to detect chemically different regions. In it, $\tau_{\rm vW}$ and $\tau_0^{\rm TF}$ are the von Weizsäcker

$$\tau_{\rm vW}:=\frac{|\nabla n|^2}{8n} \tag{68}$$

and Thomas–Fermi

$$\tau_0^{\mathrm{TF}} := \frac{3}{10}\left(3\pi^2\right)^{2/3} n^{5/3} \equiv c_0 n^{5/3} \tag{69}$$

kinetic energy densities respectively. Details of other indicators (e.g. $z := \tau_{\mathrm{vW}}/\tau_{\mathrm{s}}$) [78] are un-needed in this discussion.

Putting aside the orbital-dependence itself for a moment, generalization to $\mathrm{T} > 0$ K raises obvious questions. In α, for example, should the ground state TF KE density be retained or should it be replaced by $\tau_{\mathrm{s}}^{\mathrm{TF}}(n,t)$ defined below equation (12)? One can argue that α is supposed to sense chemically different regions, so it does not matter whether the density is ground-state or thermal. The contrary argument is that $\tau_{\mathrm{s}}^{\mathrm{TF}}(n,t)$ is the more appropriate sensor for the thermal cases since it has intrinsic T dependence as well as the dependence from $n(\mathbf{r},\mathrm{T})$. Defining α with the thermal TF kinetic energy density preserves the property of the ground-state definition, that is $\alpha \approx 1$ correctly recognizing metallic regions. Moreover, it is inherently consistent with the noninteracting free-energy (and its components) functional concept. This is an example of the choices faced by functional developers.

Still in the ground-state context, the establishment of orbital-free meta-GGA XC approximations has proceeded entirely by 'de-orbitalization' of the orbital-dependent forms. In essence, that replaces the τ_{s} orbital dependence with an approximate pure density functional, dependent for numerical stability reasons (high-order spatial derivatives in the KS potential) upon n, ∇n (specifically $p := s^2$), and $\nabla^2 n$ (specifically, q). After early versions [79, 80], Mejía–Rodríguez and Trickey ('M-RT') [81–83] introduced and demonstrated a de-orbitalization protocol. Basically it is to select a high quality one-point orbital-free KEDF [15], $\tau_{\mathrm{s}}[n,\{\phi\}] \approx \tau_{\mathrm{L}}[n,s^2,q]$ and reparametrize it to give a good approximation to an orbital-dependent indicator such as α,

$$\alpha_{\mathrm{L}}\left[n,\nabla n,\nabla^2 n\right] \approx \alpha\left[\{\varphi\}\right] \tag{70}$$

for isolated atoms. (Recently the M-RT scheme was extended by Francisco *et al* [84] to treat two-indicator functionals.) (Remarks: The subscript 'L' denotes density-Laplacian dependence. As a cautionary note, both the orbital-dependent and de-orbitalized ground-state meta-GGAs have non-trivial numerical stability issues [85–87].)

Once one has a de-orbitalized ground-state meta-GGA XC functional, extension to $\mathrm{T} > 0$ is, at least in principle, possible by exploiting the $\mathrm{T} > 0$ gradient expansion for X and C. Only a little has been done on that.

With these contextual matters in hand, we turn to specifics. One route around some of the challenges of orbital-dependence and de-orbitalization is to consider an additive modification of a ground-state functional, conceptually the same approach as in equation (63) for $f_{\mathrm{xc}}^{\mathrm{addPBE}}$. For virtually any meta-GGA ground-state XC functional, one can define a general additive thermal correction [40] at the GGA level of refinement, to wit

$$\Delta\mathcal{F}_{\mathrm{xc}}^{\mathrm{GGA}}[n,\mathrm{T}] = \mathcal{F}_{\mathrm{xc}}^{\mathrm{KDT16}}[n,\mathrm{T}] - E_{\mathrm{xc}}^{\mathrm{PBE}}[n]\,, \tag{71}$$

Then the simple T-dependent meta-GGA is constructed as

$$\mathcal{F}_{\mathrm{xc}}^{\mathrm{MGGA}}[n,\mathrm{T}] = E_{\mathrm{xc}}^{\mathrm{MGGA}}[n] + \Delta\mathcal{F}_{\mathrm{xc}}^{\mathrm{GGA}}[n,\mathrm{T}]\,. \tag{72}$$

Recall from equation (62), that $\Delta\mathcal{F}_{\mathrm{xc}}^{\mathrm{GGA}}[n,\mathrm{T}] \approx 0$ at low-T, and that both the ground-state PBE and any properly constrained ground-state meta-GGA reduce to the ground-state LDA XC in the high-T limit (i.e. in the homogeneous density limit)

$$\lim_{\mathrm{T}\to\infty} E_{\mathrm{xc}}^{\mathrm{MGGA}}[n] \approx E_{\mathrm{xc}}^{\mathrm{LDA}}[n]\,, \tag{73}$$

and

$$\lim_{\mathrm{T}\to\infty} E_{\mathrm{xc}}^{\mathrm{PBE}}[n] \approx E_{\mathrm{xc}}^{\mathrm{LDA}}[n]\,. \tag{74}$$

The implication of these two equations is that $E_{\mathrm{xc}}^{\mathrm{MGGA}}[n] \approx E_{\mathrm{xc}}^{\mathrm{PBE}}[n]$ at high T. That yields the following limiting behavior of the additive thermal MGGA given in equation (72): $\mathcal{F}_{\mathrm{xc}}^{\mathrm{MGGA}}[n,\mathrm{T}] \approx E_{\mathrm{xc}}^{\mathrm{MGGA}}[n]$ at low-T and $\mathcal{F}_{\mathrm{xc}}^{\mathrm{MGGA}}[n,\mathrm{T}] \approx \mathcal{F}_{\mathrm{xc}}^{\mathrm{KDT16}}[n,\mathrm{T}]$ at high-T.

To be useful in the OF-DFT context, this thermalization scheme has to be applied to an orbital-independent meta-GGA. The specific example [40] is the thermal adaptation of the de-orbitalized

version, (SCAN-L) [81, 83], of the ground-state strongly constrained and appropriately normed SCAN functional. Denoted T-SCAN-L, an example application of orbital-free simulations employing it in conjunction with the noninteracting free-energy meta-GGA F_{τ}^{DEL} given in equation (41) is given in [34]. For He at $\rho_{He} = 0.387\ \mathrm{g\,cm^{-3}}$, the pressure error was less than 2% with respect to the combined KS and PIMC reference data for the range $7 \leqslant \mathrm{T} \leqslant 200$ eV. The additive thermalization scheme equation (72), applied to the de-orbitalized, regularized restored r^{2}SCAN-L functional [83, 88], reduces the number of SCF iterations compared to T-SCAN-L by as much as a factor of three, depending upon the material and state conditions. Such a reduction typically is related to improved numerical stability.

A technical point closely related to one we already made is relevant. The issue is avoidance of double counting of thermal contributions. For that, the additive thermal correction, equations (71) and (72), is designed to be applied to a ground-state XC functional E_{xc}. That *excludes* explicitly orbital-dependent functionals such as SCAN [69], and r^{2}SCAN [88] *unless* their Fermi–Dirac occupations (recall equation (51)) are set to $\mathrm{T} = 0$. Otherwise, use of the orbital-dependent SCAN or r^{2}SCAN in conjunction with the additive thermal correction $\Delta\mathcal{F}_{\mathrm{xc}}^{\mathrm{GGA}}$ would have an uncontrolled and uncorrectable double counting of XC thermal effects. An advantage of using the de-orbitalized versions [81, 83] is that they automatically avoid this problem because they do not depend upon τ_{s}.

At this writing, the development of a full XC free-energy meta-GGA is being undertaken by the authors. The analysis and construction is the XC counterpart of the noninteracting meta-GGA development surveyed in section 3.3. However, there are subtle and sometimes difficult differences. Initial indications suggest that the change in calculated results relative to those from the additive meta-GGA just described may not be large. Whatever the case, when completed, the product will be an orbital-dependent XC free-energy functional. De-orbitalization or some related orbital-free conversion will be required for use in $\mathrm{T} > 0$ OF-DFT simulations.

5. Limitations and challenges

There are two significant issues for free-energy OF-DFT that are comparatively undiscussed. One, non-additivity, is implicated by the other, the virtually inescapable use of LPPs.

5.1. AE LPPs

Most of the popular conventional-KS and OF-DFT codes for extended system calculations use a plane-wave basis. Compelling reasons include the freedom from Pulay forces in AIMD and the systematic straight-forwardness by which the basis may be enriched. As has long been known, the singular bare-Coulomb electron-nuclear attraction cannot be treated efficiently in the plane-wave basis. The problem is alleviated by use of pseudo-potentials. They have a long, rich history, including 'non-local' pseudo-potentials which in fact introduce an orbital dependence in otherwise ordinary ground-state KS calculations. OF-DFT, however, requires pseudo-potentials without any orbital dependence, i.e. LPPs that describe the electron–ion interaction by a local multiplicative function. (Remark: Some more sophisticated approaches, such as the projector augmented-wave (PAW) based [89] and angular-momentum-dependent OF-DFT [90] have been proposed. But they remain largely exploratory and not used widely. There is, however, an important PAW result that we discuss below.)

Simulations at high T and or P necessitate AE LPPs. The reasoning begins with near-ambient conditions. For them, deep core electron densities ([He]- and [Ne]-core for second and third row elements respectively) can be considered frozen and excluded from consideration. That leads to smooth LPPs, hence rather smooth weakly-inhomogeneous valence-electron pseudo-densities. As was noticed in several references [15, 23, 34], many semi-local and non-local orbital-free functionals are tied to or constructed with respect to HEG properties. Those functionals should be reasonably accurate for systems with such valence pseudo-densities.

But clearly such valence-only (or frozen-core) LPPs are not transferable to high T and P conditions. In such state conditions, temperature and/or pressure-induced ionization is inescapable, hence even the deep core electrons cannot be approximated as frozen. Two questions therefore arise: how to construct reliable AE LPPs and what is their effect when used with approximate free-energy OF-DFT functionals?

About the first question, we summarize two procedures. First, [44] provides a norm-conserving (NC) regularization that preserves the electronic density normalization inside and outside the cutoff volume, and provides a smooth AE LPP. Its first step is numerical solution of the Thomas–Fermi equation with a bare-Coulomb electron–nucleus potential for an atom in a spherical cavity (with volume corresponding to the specified material density) at given temperature. That yields a radial electron density $n(r)$. A pseudo-density $\tilde{n}(\mathbf{r})$ then is constructed by imposing a smooth analytic form inside the cutoff volume, and

requiring $\tilde{n} = n$ outside that volume, to wit

$$\tilde{n}(r) = \begin{cases} \frac{1}{4\pi} \exp\left(a + br^2 + cr^4\right), & r < r_c \\ n(r), & r \geqslant r_c \,. \end{cases} \tag{75}$$

The coefficients a, b and c are determined by enforcing the continuity of $\tilde{n}(r)$ and its radial derivative $\tilde{n}'(r)$ at $r = r_c$ and enforcing density conservation, $\int \mathrm{d}r r^2 \tilde{n}(r) = \int \mathrm{d}r r^2 n(r)$. The screened electron–ion potential is computed by inversion of the TF equation, and the NC LPP ('NC' LPP) is extracted by subtracting the Hartree term (and the XC term as well if it was included initially).

These AE NC LPPs are expected to be accurate for circumstances in which both valence electrons and typically some core electrons are totally or partially ionized. However, the well-known inability of the TF functional to reproduce atomic shell structure suggests that the procedure might be unreliable at lower- and/or P. (Remark: We are unaware of any investigation of the suitability of the NC-LPPs for use with functionals with density Laplacian q dependence.)

A more refined local pseudopotential introduced by Hartwigsen, Goedecker, and Hutter (HGH) [91] uses the so-called dual-space Gaussian form

$$v_{\mathrm{loc}}(r) = \frac{-Z_{\mathrm{ion}}}{r} \operatorname{erf}\left(\frac{r}{\sqrt{2} r_{\mathrm{loc}}}\right) + \exp\left[-\frac{1}{2}\left(\frac{r}{r_{\mathrm{loc}}}\right)^2\right] \quad \left[C_1 + C_2\left(\frac{r}{r_{\mathrm{loc}}}\right)^2 + C_4\left(\frac{r}{r_{\mathrm{loc}}}\right)^4 + C_6\left(\frac{r}{r_{\mathrm{loc}}}\right)^6\right]. \tag{76}$$

For the AE case, Z_{ion} equals the physical atomic number Z, r_{loc} is a parameter set by hand according to the required hardness (and eventual accuracy), and C_1, C_2, C_4, and C_6 are found by minimization of the differences between eigenvalues and charges within an atomic sphere for the bare-Coulomb atom and the AE pseudo-atom. A convenient special property of the dual-space Gaussian form for plane-wave codes is that there also is an analytic reciprocal space representation.

The majority of OF-DFT simulations employ valence-only LPPs. We are aware of comparatively few exceptions. AE NC LPPs were employed for OF-DFT (with the Thomas–Fermi functional) simulations of dense boron plasmas [45] and dense He-Fe and D-Cu mixtures [92]. A combination of conventional KS and OF-DFT methodology was used to generate a wide range of EOS tables for materials relevant to ICF [93–95]. The conventional KS calculations used PAW data sets and the OF-DFT used NC LPPs.

It also can be useful to represent the numerical NC LPP in the HGH analytical form. A fitting procedure that provides such a representation was developed recently. A combined set of soft and hard AE LPPs (NC and HGH LPPs respectively) transferable to extreme conditions was employed in OF-DFT AIMD simulations to establish a wide-range EOS table for a CHON quaternary compound, a new ablator material developed for laser-direct-drive targets [96].

The qualitative differences in LPPs can be quite striking. Figure 5 compares a one-electron ($1e^-$) bulk-derived local pseudopotential (BLPS) [97], two HGH $3e^-$ LPPs with different cutoffs ($r_{\mathrm{loc}} = 0.40$ and $r_{\mathrm{loc}} = 0.28$, details in [91]), and an AE NC LPP for Li. The valence-only BLPS is repulsive at $r \lesssim 0.7$ bohr, then approaches $-1/r$ Coulomb behavior at $r \gtrsim 2$ bohr. Thereby the valence pseudo-orbitals are assured to match the AE valence orbitals in the interstitial region of a bulk system. In contrast, the AE LPPs are negative in the core region. That provides smooth regularization of the Coulomb singularity. They approach the $-3/r$ bare-Coulomb behavior at $r \gtrsim 1$ (soft HGH) and $r \gtrsim 0.6$ (hard NC and HGH) bohr.

Figure 6 compares the electron density from orbital-free calculations with the one-electron BLPS and the AE soft HGH LPP (both as shown in figure 5). The calculations used the LKT GGA noninteracting free-energy functional, equation (27), combined with the ground-state LDA XC for bcc-Li with two atoms in the simulation cell, $\rho_{\mathrm{Li}} = 0.60\ \mathrm{g\,cm^{-3}}$ (lattice constant 3.3743 Å) at room temperature. The density is shown along the line connecting two Li atoms (body diagonal).

In the high-T (or high P) limit, the electron density from calculations with AE LPPs becomes smooth (weakly-inhomogeneous) because of ionization processes. In the near-ambient conditions applicable to figure 6 however, the core-electron contribution to the total electron density is sharp. As expected therefore, in these calculations, the AE density has sharp peaks that correspond to core-electron contributions at the atomic positions. But the one-electron LPP pseudo-density is very smooth, with largest values up to $10^{-2}\ \mathrm{Å^{-3}}$ primarily in the interstitial region, and almost vanishing contributions near the ion locations. The repulsive part of the BLPS LPP at $r \lesssim 0.7$ bohr shown in figure 5 causes this, with a very small magnitude in the extended valence region not exceeding $0.0085\ \mathrm{Å^{-3}}$. Such a smooth pseudo-density can be characterized as weakly-inhomogeneous, a property not true for the AE density.

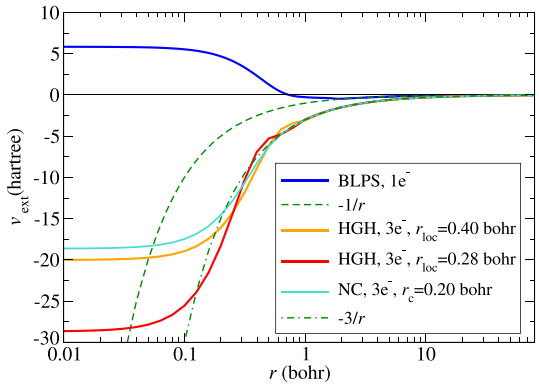

Figure 5. Local pseudopotentials for Li: one-electron bulk derived local pseudopotential (BLPS) [97], two Hartwigsen–Goedecker–Hutter (HGH) all-electron local pseudopotentials [91] with $r_{\rm loc} = 0.40$ bohr, and $r_{\rm loc} = 0.28$, and an all-electron norm conserving (NC) with $r_{\rm c} = 0.20$ bohr derived for near-ambient conditions, $\rho_{\rm Li} = 0.60$ g cm^{-3} and $T = 0.5$ eV.

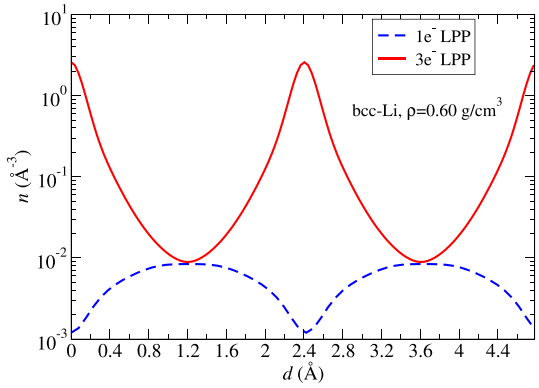

Figure 6. Electron density n for bcc-Li (cubic cell, $\rho = 0.60$ g cm^{-3}) along the line connecting two atoms on the body diagonal from OFDFT/LKT/LDA calculations with $1e^-$ and $3e^-$ LDA local pseudopotentials shown in figure 5—BLPS and HGH with $r_{\rm loc} = 0.40$ bohr respectively.

Before proceeding, it is fitting to note that there have been at least a few efforts to accommodate the orbital-dependence of non-local pseudo-potentials within the OF-DFT context. Three papers are particularly relevant.

In the first, [98] a core-like region is defined around each ionic site and the density is partitioned spatially in those spheres and the interstitial region. The sphere radii are chosen such that the non-local part of the pseudo-potential vanishes inside or at the sphere surfaces. (This is akin in concept to muffin-tin methods but without their priority on touching spheres.) A small basis expansion of the core states then is used, with the rest of the system handled by a conventional KEDF, in the case of [98], a two-point functional.

Xu *et al* [99] proceed somewhat differently. They write the non-LPP energy in terms of the KS orbitals and 1-matrix. The 1-matrix is approximated in turn by a Gaussian-based Taylor expansion to second-order that depends on the conventional KS KE density. That is de-orbitalized (though the paper does not use that term) by replacement with an OF-DFT KEDF. The short-ranged nature of the non-local terms in the pseudo-potential then leave a double integral over that non-zero domain of the local atomic-like functions and the orbital-free approximate 1-matrix. Again the Wang-Teter kernel was used for the non-local part of the KEDF.

For the purposes of the present discussion, these brief summaries suffice to focus attention on the need for some way to calculate core corrections that avoid problems of nonlinearity of the noninteracting and XC free energies (and their T = 0 counterparts).

However, there is a third study that bears directly on the main topic of this section, namely the issue of AE LPPs. In [89], Lehtomäki *et al* devised a way to use PAWs with OF-DFT. The advantage of that combination is that it provides AE values for calculated quantities such as bond lengths, lattice constants, and cohesive energies. We are careful here to make a distinction highlighted by those authors. The PAW scheme is not an AE *method* in the conventional sense of the term, but it does yield highly accurate approximate AE *values* for the physical observables. With the real-space grid code GPAW, the TFλvW KEDF

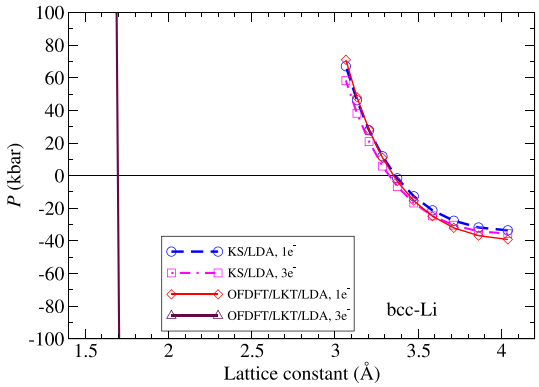

Figure 7. Pressure as a function of lattice constant as predicted by conventional KS- and OF-DFT (with $1e^-$ and $3e^-$ LDA local pseudopotential) for bcc-Li at T = 300 K. OF calculations are performed with LKT/GGA noninteracting functional in combination with the ground-state LDA XC. It also was used in the conventional KS scheme.

($T_s \approx T_{TF} + \lambda T_W$; $0 \leqslant \lambda \leqslant 1$; in this case $\lambda = 1$) and the PBE XC functional, they found that the AE lattice constant for bcc Li was far smaller than the results from LPP calculations reported in [49], 1.65 Å versus 3.43 Å. Moreover, the AE bulk modulus was huge (945 GPa) compared to the LPP result (14.9 or 15.2 GPa depending on LPP details). The PAW itself is not in doubt. Conventional KS calculations with it give sensible lattice parameter and bulk modulus values. Clearly something very peculiar is happening with the LPPs.

5.2. Implications of noninteracting kinetic energy nonadditivity

The qualitative differences in pseudo-densities have drastic consequences for OF-DFT prediction accuracy. Even with regularized potentials, the pseudo-orbitals for deep core electrons are not smooth. It therefore is common practice to treat the core electrons as 'frozen', hence without an active role in the conventional KS or OF-DFT minimization problem. Irrespective of conventional KS or OF-DFT, T = 0 or > 0, the total electron density can be split into core ('c') and valence ('v') electron densities

$$n(\mathbf{r}) = n_c(\mathbf{r}) + n_v(\mathbf{r}) \,. \tag{77}$$

Written in terms of KS orbitals, this is $n_c(\mathbf{r}) = \sum_{i=1}^{N_c} f_i |\varphi_i(\mathbf{r})|^2$ and $n_v(\mathbf{r}) = \sum_{i=N_c+1}^{N_e} f_i |\varphi_i(\mathbf{r})|^2$. As before, the f_i and φ_i are the KS occupations and orbitals respectively. For second and third row atoms, $N_c = 2$ ([He]-core) and 10 ([Ne]-core) respectively. Extension and more options for higher-Z atoms are obvious.

This rather intuitively sensible decomposition introduces a problem. To illustrate we performed a set of static calculations for bcc-Li and fcc-Al with conventional KS and OF-DFT methods employing two types of pseudo-potentials, valence-only and AE. Figure 7 shows pressure as a function of lattice constant for bcc-Li. The equilibrium lattice constants predicted by conventional KS and OF-DFT calculations with the one-electron ('$1e^-$') LPP are nearly identical, close to 3.37 Å. The conventional KS $3e^-$ LPP equilibrium lattice constant is a little bit smaller, ≈3.33 Å. But the OF-DFT simulations with the AE LPP gives a dramatically smaller value, 1.7 Å.

This is precisely the same misbehavior found earlier by Lehtomäki *et al* [89] that was discussed above. It confirms the remark made there. The gross misbehavior is rooted in the qualitative difference between AE and valence-only LPPs.

The situation for fcc-Al is quite similar. See figure 8. The KS equilibrium lattice constants from calculations with PBE XC, frozen [Ne]-core PAW, and an AE LPP are ≈4.04 Å. The OF-DFT prediction with a $3e^-$ LPP predicts a slightly overestimated value, ≈4.14 Å. But for OF-DFT with the AE ('$13e^-$') LPP, the system collapses to ≈2.5 Å lattice parameter.

These drastic equilibrium lattice constant differences as predicted by OF-DFT with valence-only versus AE LPPs are a direct consequence of the noninteracting kinetic energy nonadditivity. We continue with the zero-temperature case for simplicity. Extension to T > 0 K is basically straightforward.

The explicit KS kinetic energy is additive with respect to core and valence orbitals

$$T_s^{KS}\left[\{\varphi_i\}_{i=1}^{N_e}\right] = T_s^{KS}\left[\{\varphi_i\}_{i=1}^{N_c}\right] + T_s^{KS}\left[\{\varphi_i\}_{i=N_c+1}^{N_e}\right] \tag{78}$$

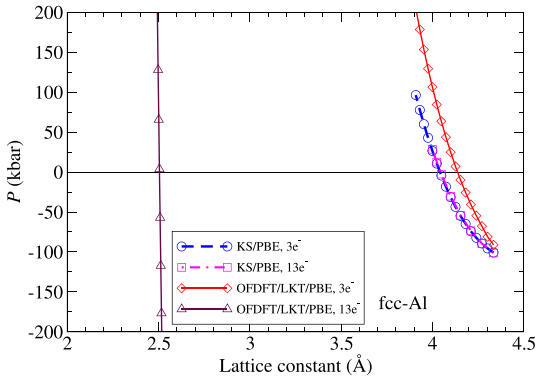

Figure 8. Pressure for fcc Al as a function of lattice constant as predicted by conventional KS-DFT (with $3e^-$ PBE PAW and 13^- PBE local pseudopotential) and OF-DFT (with $3e^-$ and $13e^-$ PBE local pseudopotential). All calculations used PBE XC.

but *not* with respect to the density decomposition in equation (77). Instead, because the orbital-free representation of the KS kinetic energy is nonlinear in the density (recall the Thomas–Fermi KE density $\propto n^{5/3}$), one has

$$T_{\rm s}^{\rm OF}[n] = T_{\rm s}^{\rm OF}[n_{\rm c}] + T_{\rm s}^{\rm OF}[n_{\rm v}] + T_{\rm s,nadd}^{\rm OF}[n_{\rm c}, n_{\rm v}]\,. \tag{79}$$

The nonadditive kinetic energy $T_{\rm s,nadd}^{\rm OF}[n_{\rm c}, n_{\rm v}]$ is zero only if the core and valence electron densities do not overlap.

Because the XC functional also is nonlinear in the density (Slater LDA is $\propto n^{4/3}$), it also is nonadditive:

$$E_{\rm xc}^{\rm DFT}[n] = E_{\rm xc}^{\rm DFT}[n_{\rm c}] + E_{\rm xc}^{\rm DFT}[n_{\rm v}] + E_{\rm xc,nadd}^{\rm DFT}[n_{\rm c}, n_{\rm v}]\,. \tag{80}$$

Given all this, for the case of a valence-only pseudo-potential $v_{\rm ext}^{\rm ps}$, the total KS energy takes the form

$$E^{\rm KS,ps}[n_{\rm v}] = T_{\rm s}^{\rm KS}[n_{\rm v}] + E_{\rm H}[n_{\rm v}] + E_{\rm xc}[n_{\rm v}] + \int n_{\rm v}(\mathbf{r})\, v_{\rm ext}^{\rm ps}(\mathbf{r})\,{\rm d}\mathbf{r} + E_{\rm ion}(\{\mathbf{R}\})\,. \tag{81}$$

with $T_{\rm s}^{\rm KS}[n_{\rm v}]$ being the second term in equation (78).

The difference between the AE and pseudo-potential total energies, equations (1) and (81) respectively, is

$$\begin{aligned}\Delta E^{\rm KS} = {} & T_{\rm s}^{\rm KS}\left[\{\varphi_i\}_{i=1}^{N_{\rm c}}\right] + E_{\rm xc}^{\rm DFT}[n_{\rm c}] + E_{\rm xc,nadd}^{\rm DFT}[n_{\rm c}, n_{\rm v}] + \int n_{\rm c}(\mathbf{r})\, v_{\rm ext}(\mathbf{r})\,{\rm d}\mathbf{r} \\ & + \int n_{\rm v}(\mathbf{r})\left(v_{\rm ext}(\mathbf{r}) - v_{\rm ext}^{\rm ps}(\mathbf{r})\right){\rm d}\mathbf{r} + E_{\rm H}[n_{\rm c}] + E_{\rm H,nadd}[n_{\rm c}, n_{\rm v}]\,,\end{aligned} \tag{82}$$

where

$$E_{\rm H,nadd}[n_{\rm c}, n_{\rm v}] = \int\int \frac{n_{\rm c}(\mathbf{r})\, n_{\rm v}(\mathbf{r}')}{|\mathbf{r}-\mathbf{r}'|}{\rm d}\mathbf{r}{\rm d}\mathbf{r}'\,. \tag{83}$$

Though the deep core-electron levels have much lower energy in comparison to the valence levels, they cannot be considered as independent of the local environment. Core levels are affected by on-site valence-electron orbital changes. As a consequence, changes in the individual terms in equation (82) might be large. However, pseudopotential methods with active valence electrons only, which neglect any changes of core levels, are surprisingly quite accurate relative to the fully self-consistent results. Von Barth and Gelatt [100] demonstrated that the energy difference equation (82) has only a weak dependence on the local environment (i.e. it is near-constant) because of cancellation of large errors involved in the frozen-core approximation implicitly used by pseudo-potential methods. They showed that the $\Delta E^{\rm KS}$ changes vanish to first order in the core-charge-density difference (see details in [100]).

The nonadditive XC term (third term) in equation (82) depends on the valence electron density, hence upon interactions with neighboring atoms. Therefore $E_{\rm xc,nadd}$ introduces an additional error associated with the pseudo-potential calculations. Because the magnitude of the XC energy typically is about 10% of the total energy, however, the $E_{\rm xc,nadd}$ error typically is small.

The seventh term, $E_{{\rm H},nadd}$, is due as well to nonadditivity, but it does not introduce additional errors as the corresponding functional derivative, $v_{\rm H}([n];\mathbf{r}) = \delta E_{\rm H}[n]/\delta n(\mathbf{r})$, is linear with respect to density.

The total orbital-free pseudo-potential energy, in parallel with equation (81), is

$$E^{\mathrm{OF,ps}}\left[n_{\mathrm{v}}\right]=T_{\mathrm{s}}^{\mathrm{OF}}\left[n_{\mathrm{v}}\right]+E_{\mathrm{H}}\left[n_{\mathrm{v}}\right]+E_{\mathrm{xc}}\left[n_{\mathrm{v}}\right]+\int n_{\mathrm{v}}\left(\mathbf{r}\right)v_{\mathrm{ext}}^{\mathrm{ps}}\left(\mathbf{r}\right)d\mathbf{r}+E_{\mathrm{ion}}\left(\{\mathbf{R}\}\right). \tag{84}$$

The orbital-free counterpart of equation (82), i.e. the difference between the AE and pseudo-potential OF energies, is

$$\begin{aligned}\Delta E^{\mathrm{OF}}=&T_{\mathrm{s}}^{\mathrm{OF}}\left[n_{\mathrm{c}}\right]+E_{\mathrm{xc}}^{\mathrm{DFT}}\left[n_{\mathrm{c}}\right]+E_{\mathrm{xc,nadd}}^{\mathrm{DFT}}\left[n_{\mathrm{c}},n_{\mathrm{v}}\right]+T_{\mathrm{s,nadd}}^{\mathrm{OF}}\left[n_{\mathrm{c}},n_{\mathrm{v}}\right]+\int n_{\mathrm{c}}\left(\mathbf{r}\right)v_{\mathrm{ext}}\left(\mathbf{r}\right)\mathrm{d}\mathbf{r}\\&+\int n_{\mathrm{v}}\left(\mathbf{r}\right)\left(v_{\mathrm{ext}}\left(\mathbf{r}\right)-v_{\mathrm{ext}}^{\mathrm{ps}}\left(\mathbf{r}\right)\right)\mathrm{d}\mathbf{r}+E_{\mathrm{H}}\left[n_{\mathrm{c}}\right]+E_{\mathrm{H,nadd}}\left[n_{\mathrm{c}},n_{\mathrm{v}}\right].\end{aligned} \tag{85}$$

Equation (85) includes all the terms in the KS energy difference equation (82), with the exception that the fourth term arises only in the orbital-free approach. The XC nonadditivity arguments do not hold for it because the noninteracting KE has the same order of magnitude as the total energy (recall the Coulomb virial theorem). Hence, $|T_{\mathrm{s,nadd}}^{\mathrm{OF}}[n_{\mathrm{c}},n_{\mathrm{v}}]|\gg|E_{\mathrm{xc,nadd}}^{\mathrm{DFT}}[n_{\mathrm{c}},n_{\mathrm{v}}]|$, and changes of this term associated with the local environment might introduce large errors.

Detailed comparative study of these two terms is a matter of current investigation. However, at the least one can conclude that the use of pseudo-potentials with frozen core (or valence-only) in OF-DFT simulations is not soundly justified unless some kind of nonlinear kinetic energy core correction is made. The relatively good accuracy of orbital-free approximations for simulations with such valence-only pseudo-potentials (e.g. the $3e^{-}$ LPP calculation on fcc Al discussed above) is strongly suggestive of error cancellation between the orbital-free approximate KEDF calculation and the omission of nonlinear KE core correction. Transitioning to the AE framework, as needed for WDM calculations, removes the technical need for the nonlinear KE core correction but exposes the major error in a simple approximate KEDF.

OF-DFT (both ground-state and finite T) thus is confronted with a challenge. Introduction of a nonlinear core correction for the kinetic energy likely will harm rather than help the accuracy of OF-DFT computations with currently available noninteracting functionals, hence necessitating the development of new approximate noninteracting functionals.

5.3. Nonlinear core corrections

Having nonlinear core corrections for the kinetic energy would be useful, at minimum, as a means for avoiding the use of AE LPPs under many T,*P* conditions. This appears to be a priority need for OF-DFT progress. There is precedent in the context of construction of pseudo-potentials with nonlinear XC core corrections. We sketch that here.

A simple scheme is the nonlinear core correction proposed by Louie *et al* [101]. It constructs a 'partial core density' $n_{\mathrm{core}}^{\mathrm{partial}}(r)$ which is added to the valence density n_{v} in the computation of the XC energy during the unscreening step of pseudopotential generation.

The original partial core density form was

$$n_{\mathrm{core}}^{\mathrm{partial}}\left(r\right)=\begin{cases}\frac{\sin(br)}{r}, & r<r_{\mathrm{core}}\\ n_{\mathrm{core}}\left(r\right), & r\geqslant r_{\mathrm{core}},\end{cases} \tag{86}$$

such that $n_{\mathrm{core}}^{\mathrm{partial}}(r)$ was by construction equal to the true core density outside a core cutoff radius r_{core}. That typically was a smaller cutoff radius than used for the entire pseudopotential r_{c}. Within r_{core}, the functional form equation (86) is a matter of mathematical convenience with parametrization to enforce a match between the value and gradient of $n_{\mathrm{core}}^{\mathrm{partial}}(r)$ and $n_{\mathrm{c}}(r)$ at $r=r_{\mathrm{core}}$.

The partial core density form (equation (86)) has a discontinuity in the second derivative, which precludes its use in pseudopotentials within GGA and above. Other forms are possible with continuous differentiability up to an arbitrary degree [102]. For example,

$$n_{\mathrm{core}}^{\mathrm{partial}}\left(r\right)=\begin{cases}\exp\sum_{i=0}^{7}c_{i}r^{2i}, & r<r_{\mathrm{core}}\\ n_{\mathrm{core}}\left(r\right), & r\geqslant r_{\mathrm{core}}.\end{cases} \tag{87}$$

From this sketch, it should be apparent that one route to address the nonadditivity problem of the noninteractive kinetic energy is to devise a nonlinear core KE correction.

However, inclusion of a nonlinear core correction for the kinetic energy in an OF-DFT calculation may lead simulations using frozen-core LPPs to similar results as AE LPPs (i.e. significant underestimation of lattice constants). Rather than adopting such a strategy, reformulation of the orbital-free noninteracting functionals for separable core and valence densities may be necessary. An example of the density partition into delocalized and localized parts that is treated by different orbital-free functionals is given in [103].

6. Conclusions and perspective

We have summarized key elements in progress over the last 15 years on the constraint-based development of orbital-free density approximations for noninteracting and XC free-energy functionals. Those two approximate functionals are critical ingredients for orbital-free simulations of matter at extreme conditions.

The ground-state XC 'Jacob's ladder' rung typology has been extended to both the noninteracting and XC free-energy functionals. It is important to emphasize that, as expected, higher-rung functionals generally provide improvements in accuracy as compared to the lower rungs.

Thus, the first (LDA) rung was developed in 1948 and 2014 for the noninteracting (Thomas–Fermi) and XC (KSDT) free-energy respectively. The second, fully thermal GGA rungs were developed in 2012 (noninteracting free-energy GGA-level framework) and 2018 (fully thermal KDT16 GGA XC). The constraint-based development of these two GGA rungs used similar approaches: temperature dependences are defined by analysis of the second-order gradient expansion (for noninteracting and XC free-energy respectively), reduced density gradients with explicit temperature dependence are identified from the corresponding GE2, and functional forms are defined in the usual GGA spirit.

The recently developed Laplacian (meta-GGA) level framework for noninteracting free energy functionals [34] is based on reduced density variables with T-dependences defined from the fourth-order gradient expansion for the noninteracting free-energy of a weakly inhomogeneous electron gas. So far, the meta-GGA level XC free-energy approximation is realized via an additive approach in which the thermal GGA-level correction augments a ground-state meta-GGA XC.

In all cases, both the noninteracting and XC free-energy functionals reduce to known ground-state counterparts with known performance, such that these functionals can be used across the entire range of temperatures.

Local pseudopotentials are an important ingredient for orbital-free calculations. The vulnerability of existing one-point orbital-free functionals to the limitations of pseudopotentials is an increasingly pressing problem. Valence-only pseudopotentials require relatively small energy cutoffs, and the resulting densities usually are acceptably smooth. Such LPPs in combination with currently available single-point orbital-free approximations frequently provide reasonably accurate results, especially for metals and semi-conductors.

Simulations at extreme conditions, however, require AE LPPs. Orbital-free calculations with AE LPPs at near-ambient conditions show that equilibrium lattice constants for bcc-Li and fcc-Al are strongly underestimated as compared to both conventional KS reference and valence-only OF calculations. The accuracy of the valence-only OF calculations is attributable to incomplete error cancellation between the missing nonlinear kinetic energy core correction and the approximate KEDF.

That cancellation represents one of the limitations and challenges related to the noninteracting free-energy nonadditivity. Valence-only LPPs are not transferable to high temperatures, while currently existing orbital-free approximations are highly inaccurate in conjunction with AE LPPs at low-T. A combination of the valence-only and AE LPPs in principle can be used across the temperature regimes *if* continuity of properties of interest, including thermodynamic derivatives with respect to temperature, can be provided upon the switching between LPPs.

XC nonlinear core corrections address the nonadditivity of XC functionals and thereby improve the accuracy of valence-only pseudopotentials. It appears that similar KE nonlinear core corrections can be developed for valence-only LPPs. However, we expect that the accuracy of OF calculations using current approximate functionals in conjunction with such corrected valence-only LPPs may degrade drastically, becoming closer to the accuracy of calculations with AE LPPs. Addressing that challenge almost certainly will require development of new orbital-free noninteracting functionals that treat core and valence electron densities differently. Development of machine-learning augmented orbital-free approximations also may provide new routes to development of orbital-free functionals accurate for AE calculations at a wide range of temperatures.

Data availability statement

The data cannot be made publicly available upon publication because they are not available in a format that is sufficiently accessible or reusable by other researchers. The data that support the findings of this study are available upon reasonable request from the authors.

Acknowledgments

VVK and KPH acknowledge the support by the Department of Energy [National Nuclear Security Administration] University of Rochester 'National Inertial Confinement Fusion Program' under Award Number DE-NA0004144 and U.S. National Science Foundation PHY Grant No. 2205521. This research used resources of the National Energy Research Scientific Computing Center, a DOE Office of Science User Facility supported by the Office of Science of the U.S. Department of Energy under Contract No. DE-AC02-05CH11231 using NERSC award FES-ERCAP0027845.

ORCID iDs

Valentin V Karasiev https://orcid.org/0000-0003-3445-6797
Katerina P Hilleke https://orcid.org/0000-0003-4322-8403
S B Trickey https://orcid.org/0000-0001-9224-6304

References

[1] Hohenberg P and Kohn W 1964 *Phys. Rev.* **136** B864
[2] Kohn W and Sham L J 1965 *Phys. Rev.* **140** A1133
[3] Levy M 1979 *Proc. Natl Acad. Sci.* **76** 6062
[4] Lieb E 1983 *Int. J. Quantum Chem.* **24** 243
[5] Dreizler R M and Gross E K U 1990 *Density Functional Theory: An Approach to the Quantum Many-Body Problem* (Springer)
[6] Parr R G and Yang W 1989 *Density-Functional Theory of Atoms and Molecules* (Oxford University Press)
[7] Engel E and Dreizler R M 2013 *Density Functional Theory* (Springer)
[8] Harris F E, Monkhorst H J and Freeman D L 1992 *Algebraic and Diagrammatic Methods in Many-Fermion Theory* (Oxford University Press)
[9] Shavitt I 1998 *Mol. Phys.* **94** 3
[10] Bartlett R and Musial M 2007 *Rev. Mod. Phys.* **79** 291
[11] Shavitt I and Bartlett R 2009 *Many-Body Methods in Chemistry and Physics* (Cambridge University Press)
[12] Bartlett R J 2011 Wiley Interdiscip. Rev.-Comput. Mol. Sci. **2** 126
[13] Stephens P, Devlin F, Chabalowski C and Frisch M 1994 *J. Phys. Chem.* **98** 11623
[14] Teale A M *et al* 2022 *Phys. Chem. Chem. Phys.* **24** 28700
[15] Mi W, Luo K, Trickey S B and Pavanello M 2023 *Chem. Rev.* **123** 12039
[16] Becker A, Bethkenhagen M, Kellermann C, Wicht J and Redmer R 2018 *Astron. J.* **156** 149
[17] Graziani F, Desjarlais M P, Redmer R and Trickey S B 2014 *Frontiers and Challenges in Warm Dense Matter* vol 96 (Springer)
[18] Mermin N D 1965 *Phys. Rev.* **137** A1441
[19] Cytter Y, Rabani E, Neuhauser D and Baer R 2018 *Phys. Rev.* B **97** 115207
[20] Zhang S, Wang H, Kang W, Zhang P and He X T 2016 *Phys. Plasmas* **23** 042707
[21] Blancheta A, Clérouin M, Torrent J and Soubiran F 2022 *Comput. Phys. Commun.* **271** 108215
[22] Sadigh B, Åberg D and Pask J 2023 *Phys. Rev.* E **108** 045204
[23] Karasiev V V, Mihaylov D I, Zhang S, Hinz J P, Goshadze R M N and Hu S X 2024 *Phys. Plasmas* **31** 072702
[24] Karasiev V V, Sjostrom T and Trickey S B 2014 *Comput. Phys. Commun.* **185** 3240
[25] Karasiev V, Chakraborty D, Dufty J, Harris F, Runge K and Trickey S B 2014 *Frontiers and Challenges in Warm Dense Matter* ed F Graziani, M Desjarlais, R Redmer and S B Trickey (Springer) pp 61–85
[26] Medvedev M, Bushmarinov I, Sun J, Perdew J and Lysenko K 2017 *Science* **355** 49
[27] Feynman R P, Metropolis N and Teller E 1949 *Phys. Rev.* **75** 1561
[28] Perrot F 1979 *Phys. Rev.* A **20** 586
[29] Karasiev V V, Sjostrom T and Trickey S B 2012 *Phys. Rev.* B **86** 115101
[30] Karasiev V V, Chakraborty D, Shukruto O A and Trickey S B 2013 *Phys. Rev.* B **88** 161108(R)
[31] Sjostrom T and Daligault J 2014 *Phys. Rev. Lett.* **113** 155006
[32] Luo K, Karasiev V V and Trickey S B 2020 *Phys. Rev.* B **101** 075116
[33] Ma C, Chen M, Xie Y, Xu Q, Mi W, Wang Y and Ma Y 2024 *Phys. Rev.* B **110** 085113
[34] Karasiev V V, Hinz J and Goshadze R M N 2024 *J. Phys. Chem. Lett.* **15** 8272
[35] Karasiev V V, Sjostrom T, Dufty J and Trickey S B 2014 *Phys. Rev. Lett.* **112** 076403
[36] Karasiev V V, Dufty J W and Trickey S B 2018 *Phys. Rev. Lett.* **120** 076401
[37] Sjostrom T and Daligault J 2014 *Phys. Rev.* B **90** 155109
[38] Groth S, Dornheim T, Sjostrom T, Malone F D, Foulkes W M C and Bonitz M 2017 *Phys. Rev. Lett.* **119** 135001
[39] Dornheim T, Groth S and Bonitz M 2018 *Phys. Rep.* **744** 1
[40] Karasiev V V, Mihaylov D I and Hu S X 2022 *Phys. Rev.* B **105** L081109
[41] Karasiev V V, Trickey S B and Dufty J W 2019 *Phys. Rev.* B **99** 195134
[42] Zérah G, Clérouin J and Pollock E L 1992 *Phys. Rev. Lett.* **69** 446
[43] Clérouin J, Pollock E L and Zérah G 1992 *Phys. Rev.* A **46** 5130
[44] Lambert F, Clérouin J and Zérah G 2006 *Phys. Rev.* E **73** 016403
[45] Mazevet S, Lambert F, Bottin F, Zérah G and Clérouin J 2007 *Phys. Rev.* E **75** 056404
[46] Danel J-F and Kazandjian L 2015 *Phys. Rev.* E **91** 013103
[47] Shemyakin O P, Levashov P R and Krasnova P A 2019 *Comput. Phys. Commun.* **235** 378
[48] Teller E 1962 *Rev. Mod. Phys.* **34** 627
[49] Karasiev V V and Trickey S B 2012 *Comput. Phys. Commun.* **183** 2519
[50] Karasiev V V, Sjostrom T, Dufty J and Trickey S B 2016 *Phys. Rev.* E **93** 063207
[51] Karasiev V V, Hu S X, Zaghoo M and Boehly T R 2019 *Phys. Rev.* B **99** 214110

[52] Goshadze R M N, Karasiev V V and Hilleke K P 2025 *Phys. Rev. B* submitted
[53] Perdew J P and Schmidt K 2001 *AIP Conf. Proc.* vol **577** pp 1–20
[54] Bartel J, Brack M and Durand M 1985 *Nucl. Phys.* A **445** 263
[55] Kato T 1957 *Commun. Pure Appl. Math.* **10** 151
[56] Geldart D J W and Sommer E 1985 *Phys. Lett.* A **108** 103
[57] Geldart D J W and Sommer E 1985 *Phys. Rev.* B **32** 7694
[58] Hu S X, Militzer B, Goncharov V N and Skupsky S 2011 *Phys. Rev.* B **84** 224109
[59] Wang L-W and Teter M P 1992 *Phys. Rev.* B **45** 13196
[60] Sjostrom T and Daligault J 2013 *Phys. Rev.* B **88** 195103
[61] Constantin L A, Fabiano E and Sala F D 2018 *Phys. Rev.* B **97** 205137
[62] Hilleke K P, Karasiev V V, Goshadze R M N, Trickey S B and Hu S X 2025 *Phys. Rev. Mater.* submitted
[63] Kozlowski J, Perchak D and Burke K 2023 arXiv:2308.03319
[64] Brown E W, Clark B K, DuBois J L and Ceperley D M 2013 *Phys. Rev. Lett.* **110** 146405
[65] Spink G G, Needs R J and Drummond N D 2013 *Phys. Rev.* B **085121** 88
[66] Schoof S T, Groth S, Vorberger J and Bonitz M 2015 *Phys. Rev. Lett.* **115** 130402
[67] Baker G A and Gammel J L 1970 *The Pade Approximant in Theoretical Physics* (Academic)
[68] Moldabekov Z, Schwalbe S, Böhme M P, Vorberger J, Shao X, Pavanello M, Graziani F R and Dornheim T 2024 *J. Chem. Theory Comput.* **20** 68
[69] Sun J, Ruzsinszky A and Perdew J P 2015 *Phys. Rev. Lett.* **115** 036402
[70] Dunlap E and Geldart D J W 1994 *Can. J. Phys.* **72** 1
[71] Glasser M L, Geldart D J W and Dunlap E 1994 *Can. J. Phys.* **72** 7
[72] Shegelski M R A, Geldart D J W, Glasser M L and Neilson D 1994 *Can. J. Phys.* **72** 14
[73] Geldart D J W 1996 *Nonlocal Energy Functions: Gradient Expansions and Beyond* (Springer) pp 31–55
[74] Niklasson G, Sjölander A and Singwi K S 1975 *Phys. Rev.* B **11** 113
[75] Gupta A K and Singwi K S 1977 *Phys. Rev.* B **15** 1801
[76] Karasiev V V, Chakraborty D and Trickey S B 2015 *Comput. Phys. Commun.* **192** 114
[77] Perdew J P, Burke K and Ernzerhof M 1996 *Phys. Rev. Lett.* **77** 3865
[78] Francisco H, Cancio A and Trickey S B 2023 *J. Chem. Phys.* **159** 214102
[79] Lee C, Yang W and Parr R 1988 *Phys. Rev.* B **37** 785
[80] Perdew J P and Constantin L A 2007 *Phys. Rev.* B **75** 155109
[81] Mejía-Rodríguez D and Trickey S B 2017 *Phys. Rev.* A **96** 052512
[82] Mejia-Rodriguez D and Trickey S B 2018 *Phys. Rev.* B **98** 115161
[83] Mejía-Rodríguez D and Trickey S B 2020 *Phys. Rev.* B **102** 121109
[84] Francisco H, Cancio A and Trickey S B 2024 *J. Phys. Chem.* **128** 6010
[85] Lehtola S and Marques M A L 2022 *J. Chem. Phys.* **157** 174114
[86] Bartók A P and Yates J R 2019 *J. Chem. Phys.* **150** 161101
[87] Mejía-Rodríguez D and Trickey S B 2019 *J. Chem. Phys.* **151** 207101
[88] Furness J W, Kaplan A D, Ning J, Perdew J P and Sun J 2020 *J. Phys. Chem. Lett.* **11** 8208
[89] Lehtomäki J, Makkonen I, Caro M A, Harju A and Lopez-Acevedo O 2014 *J. Chem. Phys.* **141** 234102
[90] Ke Y, Libisch F, Xia J, Wang L-W and Carter E A 2013 *Phys. Rev. Lett.* **111** 066402
[91] Hartwigsen C, Goedecker S and Hutter J 1998 *Phys. Rev.* B **58** 3641
[92] Lambert F, Clérouin J, Danel J-F, Kazandjian L and Zérah G 2008 *Phys. Rev.* E **77** 026402
[93] Hu S X, Collins L A, Goncharov V N, Kress J D, McCrory R L and Skupsky S 2015 *Phys. Rev.* E **92** 043104
[94] Ding Y H and Hu S X 2017 *Phys. Plasmas* **24** 062702
[95] Hu S X, Gao R, Ding Y, Collins L A and Kress J D 2017 *Phys. Rev.* E **95** 043210
[96] Zhang S *et al* 2022 *Phys. Rev.* E **106** 045207
[97] Zhou B, Wang Y A and Carter E A 2004 *Phys. Rev.* B **69** 125109
[98] Ke Y, Libisch F, Xia J and Carter E A 2014 *Phys. Rev.* B **89** 155112
[99] Xu Q, Ma C, Mi W, Wang Y and Ma Y 2022 *Nat. Commun.* **13** 1385
[100] von Barth U and Gelatt C D 1980 *Phys. Rev.* B **21** 2222
[101] Louie S G, Froyen S and Cohen M L 1982 *Phys. Rev.* B **26** 1738
[102] Porezag D, Pederson M R and Liu A Y 1999 *Phys. Rev.* B **60** 14132
[103] Huang C and Carter E A 2012 *Phys. Rev.* B **85** 045126